Sea Ice Morphology in the Beaufort Sea

PETER WADHAMS

Technical Report No. 36

Beaufort Sea Project

SEA ICE MORPHOLOGY IN THE BEAUFORT SEA

Peter Wadhams

Under Contract to
Ocean and Aquatic Sciences
Dept. of the Environment
512 Federal Building
1230 Government St.
Victoria, B.C., V8W 1Y4

2. Beaufort Sea Technical Report #36

1. Beaufort Sea Project.
Dept. of the Environment
512 Federal Building
1230 Government St.
Victoria, B.C., V8W 1Y4

December, 1975

CONTENTS

ACKNOWLEDGEMENTS

I wish to express my grateful thanks to the officers and crew of Maritime Command Argus 10728 for their skill and good humour; to Dr. R.E. François of Applied Physics Laboratory, University of Washington, for furnishing UARS sonar profiles; and to Mr. H. Hengeveld of Atmospheric Environment Service, Downsview, Ontario, for furnishing AES laser profiles and for assisting in their analysis.

ABSTRACT

The topography of the Beaufort Sea ice cover has been examined for the summer of 1974 and the early spring of 1975. Airborne laser profiles obtained in September and October 1974 by the Atmospheric Environment Service were analyzed, and additional flights were carried out in April, 1975 using an Argus aircraft of Maritime Command. Mean ridge heights and spacings were deduced for the elements of a grid covering much of the Beaufort Sea; in summer the mean ridge height increased linearly with the ridge frequency. For higher ridges the distributions of ridge heights in both seasons followed an identical empirical law of form $P(h) = A \exp(-Bh)$. This law was used together with ice drift information to predict extreme values of ridge height for different time intervals and spatial areas. Tentative predictions of extreme keel draft were made using reasonable factors for freeboard to draft conversion, and compared with depths at which scouring is found on the Beaufort Sea Shelf. A longitudinal profile of a sheer ridge obtained in 1972 by an unmanned arctic research submersible (UARS) of the University of Washington has been analyzed in an attempt to predict the minimum and maximum depths to be expected in a given keel linkage of known mean depth. On the basis of these and other studies of the Beaufort Sea Project a discussion is given of the extent to which sea ice deformation features may govern the long-term spread of oil under ice.

. 3

1. INTRODUCTION

This report attempts to give a quantitative description of pressure ridge and keel distributions in the Beaufort Sea. The distributions are used as a basis for speculation on how the spread of oil after an under-ice blowout may be hindered (or helped) by the ice morphology.

A general description of the ice cover in the Beaufort Sea has been given by Kovacs and Mellor (1974). It suffices here to note that the winter ice cover consists of three zones: -

Fast ice zone. A continuous sheet of normally smooth ice, stretching from the shore to anchoring points on grounded pressure ridges or ice island fragments. Its outer edge generally coincides with the 18-20 m depth contour, and its outer portions may include heavy ridging or rubble fields generated by early winter storms and subsequently "frozen in place". Detailed descriptions of this zone are given by Cooper (1974) and Stringer (1974).

Shear zone, or seasonal ice zone, found from the seaward edge of the fast ice to roughly the edge of the continental shelf. It is a zone of rapidly deforming, heavily ridged and highly irregular ice acting as a boundary layer between the circulating ice of the Beaufort Gyre and the fast ice. First-year ice predominates but with some multi-year floes and ice island fragments; this has been termed the "offshore province" by Weeks *et al* (1971).

Polar pack ice zone, extending onwards into the Arctic Basin, is in winter composed of multi-year floes with first-year ice growing and sandwiched between them. Its long-term average motion is a clockwise gyral circulation, but on a time scale of days the motion is very complex and irregular, being governed by the wind stress field.

In summer the fast ice breaks up and disperses, and an open water zone may extend up to 200 km from the coast, although it is always subject to closure when storms drive the polar pack southwards. The former shear zone is now a marginal ice zone for the polar pack and opens up considerably with many leads and polynyi.

2. RESULTS OF AES LASER PROFILING, SUMMER 1974

2.1 Technique

Laser profiles were obtained in the Beaufort Sea during the period 4 September to 7 October 1974, by Lockheed Electra aircraft CF-NAY and CF-NAZ of the Atmospheric Environment Service, Environment Canada. The instrument employed was a Spectra-Physics Geodolite 3A laser profilometer (Ketchum, 1971), in which the phase shift between amplitude-modulated beams from a CW He-Ne laser in transmissions and reflection gives the range to the reflecting target. A continuous terrain profile is obtained, which was displayed as a galvanometer light trace on ultra-violet sensitive paper. Such a recording system is not a good one from the point of view of quantitative analysis, but it permits rapid assessment of ice roughness and is therefore

. 4

relevant to the operational needs of AES. The chart record was calibrated in feet, full scale deflection corresponding to 100 feet of elevation. An example of a raw profile is shown in Fig. 1, the long-period amplitude changes being due to vertical motion of the aircraft.

The records were analyzed manually in the following way. A profile of aircraft porpoising, connecting smooth ice surfaces in a continuous curve, was drawn on to the record by hand, and the elevation of each ridge was measured relative to this profile. Ridges were ascribed to 0.5 ft. height intervals, a cut-off height of 3 feet being chosen as the minimum ridge height which can always be easily resolved against the background roughness. A broad pressure ridge especially if traversed obliquely, may display several peaks and a consistent criterion for defining an "independent ridge" is necessary so as to avoid a serious over-estimate of ridge frequency.

A criterion was devised by this author in 1972 whereby a ridge is said to be "independent" when its maximum elevation is not less than twice that of the shallowest troughs on either side of it. This is an adaptation of the Rayleigh criterion in optics, and has been employed in the analyses of under ice sonar profiles by Williams et al (1975) and of Arctic Ocean laser profiles by Lowry (1974). It is to be hoped that this or a similar criterion can be universally adopted; this would greatly facilitate the comparison of data obtained by various authors.

Navigational fixes were obtained from a Bendix doppler navigation system coupled to a MINAC 5 latitude/longitude computer (Archibald, 1972), and were recorded in the flight log every 2-5 minutes. From timing marks on the profilometer record it was then possible to identify the position of any section of record to an accuracy of approximately ±3 km. The Beaufort Sea area was divided into a grid of spacing 0° 30' in latitude and 2° 00' in longitude and the results of analyzing all sections of profile that fell within a given grid division were pooled. The grid is a fairly coarse one, but it was necessary to obtain a sufficient track length in each grid division for a valid statistical analysis.

Figure 2 shows the track sections that were analyzed, together with the intensity of coverage (number of kilometers of track in each grid division). In all, 2028 km of laser profile were analyzed; in addition, several hundred km of inshore flight data were examined but found to consist mainly of open water.

2.2 Open Water

It was possible to identify stretches of open water and young ice (ice only a few centimeters thick) because the output of a precision radiation thermometer (PRT) was displayed on the same chart record as the laser profile. A PRT measures the emission from a spot of 1° arc directly beneath the aircraft: the radiation temperature of open water was commonly 1°C above that of young ice and 2°C above that of

Fig. 1 Laser profile of Arctic sea ice.

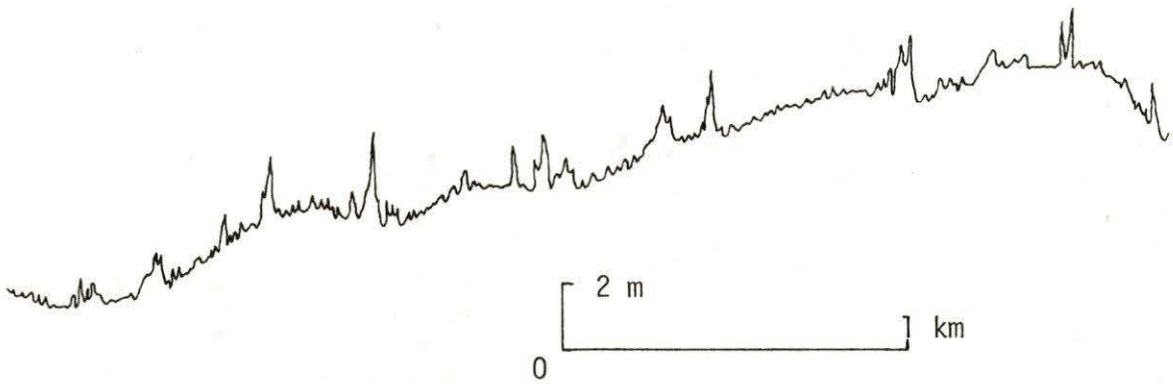

TABLE 1

Ridge Frequencies from Table 3 of Hibler et al (1974)

Ridges per km (cut-off height is 4 feet)

Region No.	Jan 12-18 '71	Mar 18-23 '71	Oct 4-6 '71	Mar 12-27 '72	Feb 6-9 '73
11	1.2	5.4		1.6	1.4
12		2.2	1.0	1.3	2.0
16	1.4			1.4	
17	0.9			0.4	2.6
18	7.6			7.8	3.3

. 6

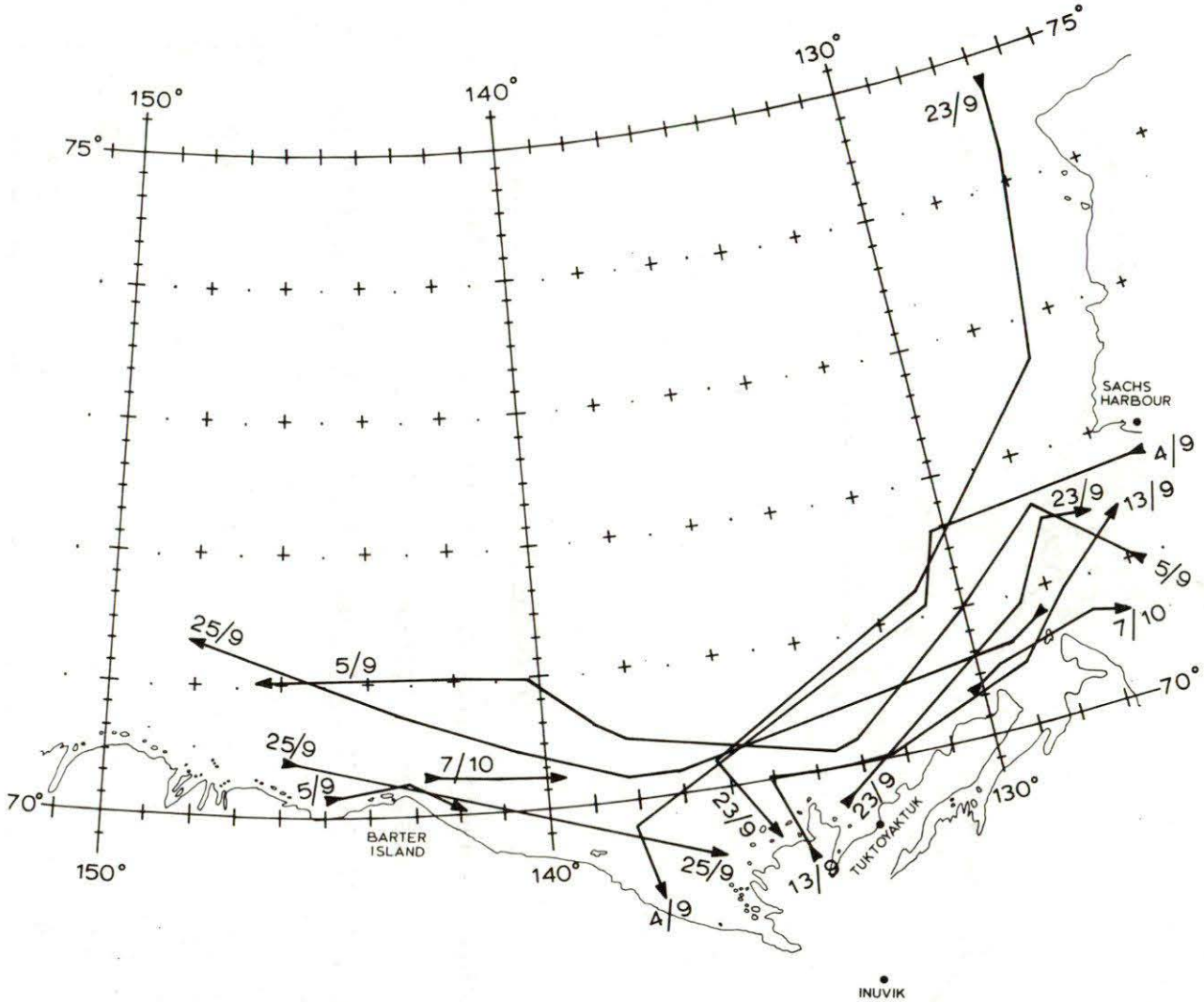

Fig. 2(a). Tracks of AES flights, summer 1974

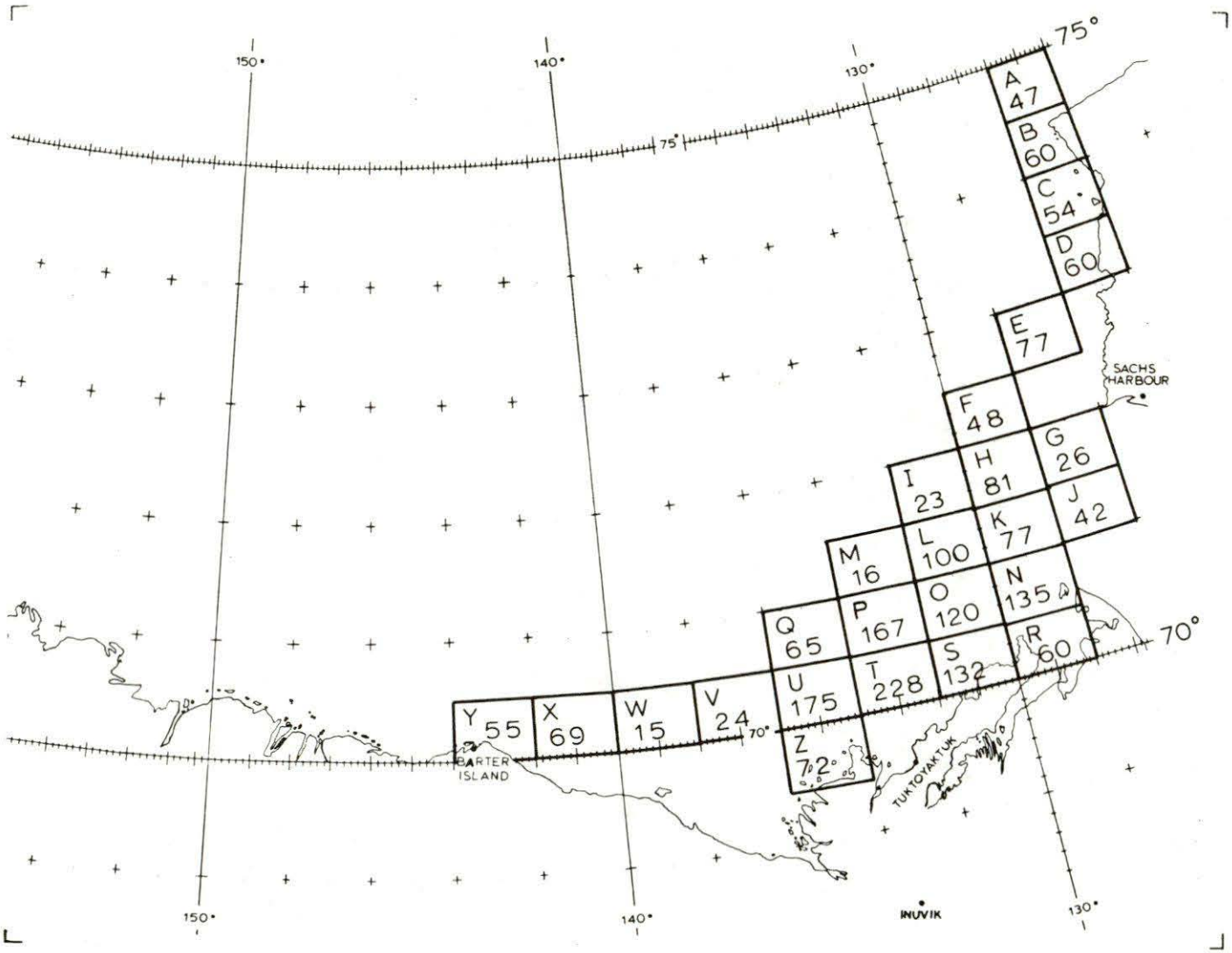

Fig. 2(b). AES, summer, 1974. Key to grid divisions, and number of km of laser profile analyzed in each.

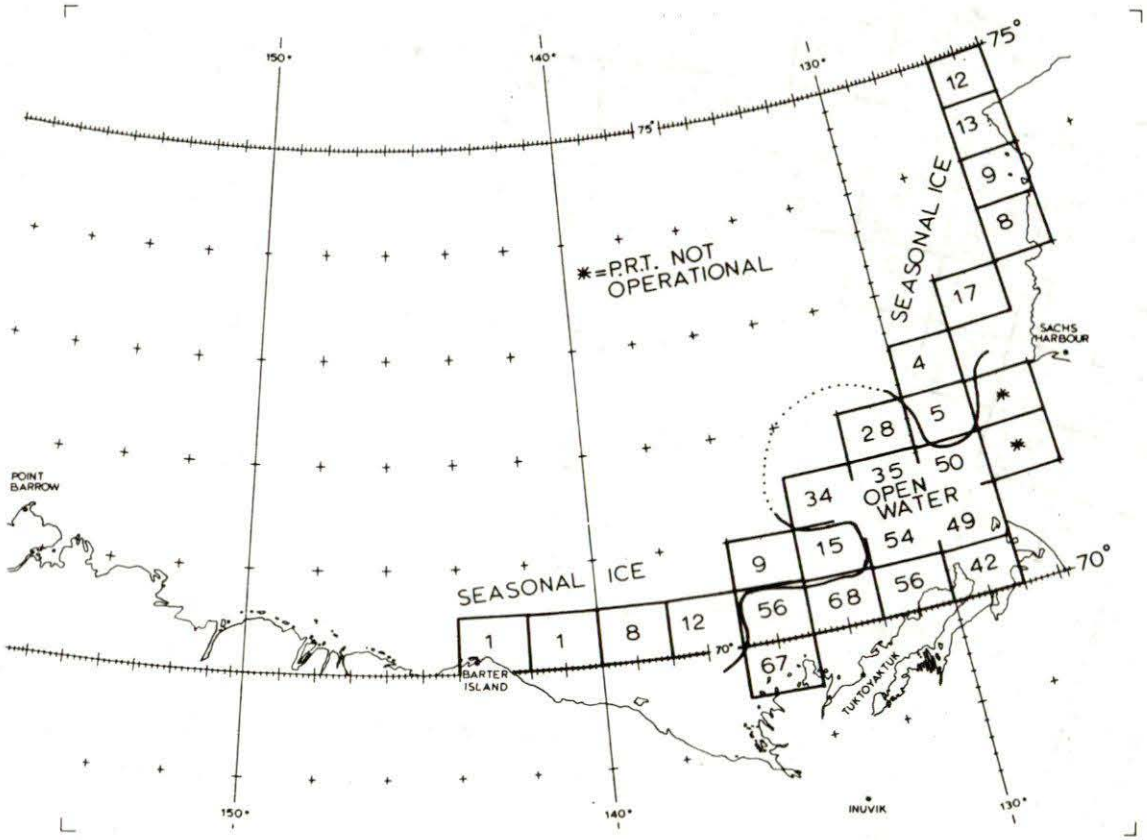

Fig. 3. Percentage of open water, Sept. - Oct., 1974.

the thicker first- and multi-year ice. This was a considerable advantage because from the laser trace the profile of waves from a wide polynya can be easily confused with the rough profile of a multi-year floe. Figure 3 shows the distribution of "open water" (defined as true open water plus young ice less than 1°C cooler than open water) over the area surveyed. The figure actually shows the percentage of track length along which open water was encountered, but if the leads and polynyi are assumed to have random orientations (Mock et al, 1972) this is an unbiased estimate of the percentage area of open water. Since the results of flights made over a five-week period were pooled, Fig. 3 is not an instantaneous picture of the extent of the ice cover, but rather it is a smoothed composite of late summer conditions. The values for the southern Beaufort Sea are therefore not very meaningful, because the percentage open water in any grid division could fluctuate greatly as the ice margin made excursions in response to the wind. However, the values for grid divisions further from shore, and particularly along the west coast of Banks Island, are of considerable interest. This represents the seasonal pack ice zone, the summer equivalent of the shear zone. In Fig. 3, thirteen grid divisions have been assigned, rather arbitrarily, to this seasonal zone, and it can be seen that, with the exception of two divisions to the north of Alaska where the ice presses in towards the land, the percentage of open water in the zone is anywhere from 5 to 17. The mean figure for the thirteen divisions is (8.7±1.4)% and if the two Alaskan areas are excluded, (10.2±1.3)%. In contrast, Wittman and Schule (1966) found less than 5% open water in winter, showing that the seasonal ice zone opens up considerably during the summer.

2.3 Frequency of Ridges

Figures 4 and 5 show the mean ridge frequency in each grid division expressed as ridges encountered per 100 km of ice cover (Fig. 4) or total laser track (Fig. 5). In each division the large number expresses the ridges per 100 km while the small number ε_1 is the probable range of accuracy, calculated from the approximate formula

$$\varepsilon_1 = \sqrt{n} \times \frac{100}{s} \qquad \ldots(1)$$

where ε_1 = standard error for number per 100 km
n = number of ridges counted along track
s = length of track in km.

Thus, from the point of view of oil spilled under a large floe, Fig. 4 shows the frequency with which ridges will be encountered within the boundaries of that floe before any leads are reached, while Fig. 5 gives the larger scale picture of ridge frequency over an average line segment of pack ice which includes leads and polynyi. Where the ice concentration is almost 100% the two figures are obviously almost the same. We find a very wide range of frequencies, but once again a clear pattern emerges. Over an area of the eastern Beaufort Sea roughly corresponding to the "seasonal zone" of Fig. 3, the ridge frequency is high, varying from 6 to over 12 per km of ice cover. Over the southeastern Beaufort Sea where the percentage of open water is high, the ridge frequency is low, about 2 to 3 per km even when corrected for open water, while in the southwestern Beaufort Sea the

. 10

frequency is similarly low despite the high concentration of ice cover.

It is instructive to compare these results with those of Hibler et al (1974), where a table of ridging intensities is presented for various parts of the Arctic Ocean and times of year. Five of the regions considered by Hibler et al fall within the Beaufort Sea area, and these have been marked on Figs. 4 and 5 with the identification numbers used by Hibler. The ridge frequencies per km (presumably of total track) are shown in Table 1. We expect these figures to be lower than our own because the cut-off height was 4 feet rather than 3. Regions 11 and 12 lie within the polar pack of the Beaufort Gyre, outside our area of measurement, and show a variable but generally low ridging intensity, the solitary summer measurement being lower still. Region 16 corresponds to our grid division T, and the frequencies are in good agreement suggesting that winter ridge frequencies can be estimated by taking the summer values for ice cover only (i.e. in winter the pack closes up but does not increase radically in ridging intensity).

The same data were analyzed independently by Tucker and Westhall (1973), using as a criterion for an independent ridge that the troughs on either side should be at least 2 feet lower than the peak (Hibler's criterion is not stated). Ridge frequencies differed by up to 20% from those given in Table 1, illustrating the importance of establishing a uniform ridge criterion. From their data Tucker and Westhall were also able to construct approximate contours of ridging intensity over the Arctic Ocean for different seasons. They show that the ridge frequency is lowest in the southern Beaufort Sea (generally less than 2 per km for ridges higher than 4 feet) and that there is not significant variation in this area with season. The highest frequency of all (8 or more per km) is found in the shear zone along the northwest border of the Canadian Archipelago, Ellesmere Island and north Greenland, and here the frequency is significantly greater in winter. The increase in frequency begins at the latitude of northern Banks Island, which is in agreement with the AES results.

2.4 Mean Height of Ridges

We now consider ridge heights. Figure 6 shows the mean ridge height in each grid division in meters, relative to a cutoff height of 0.91 m (3 ft.). Again, the small numbers ε_2 are the standard errors in each estimate, calculated by assuming a possible error of ±0.5 ft. (0.152 m) in an individual ridge height measurement. We find a wide range of mean elevations, from less than 1.2 m to almost 1.7 m, but with a concentration between 1.3 and 1.5 m, the higher values being generally found in the northernmost divisions.

Gonin (1960) found a linear positive correlation between average hummock height (for hummocks less than 0.6 m high, measured from stereo air photographs) and percentage cover of deformed ice. Hibler et al (1972) found a similar correlation between mean keel depth and number of keels per km, for under-ice sonar profiles.

. 11

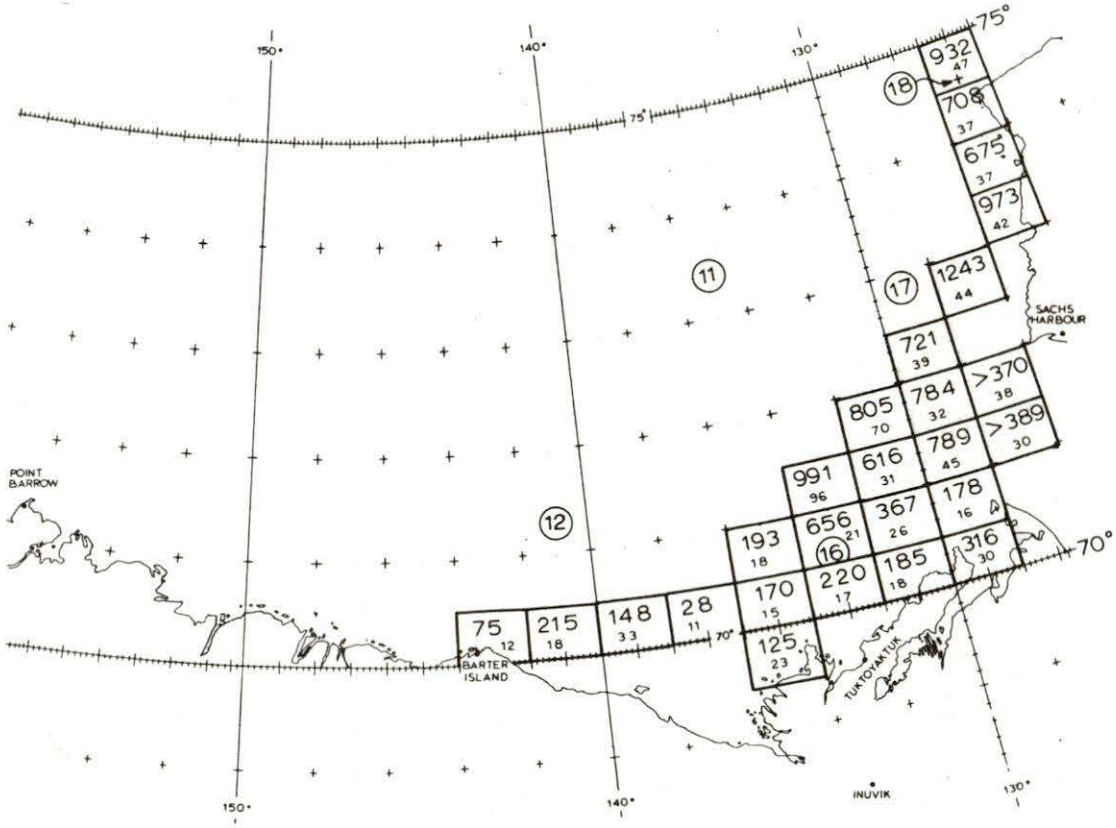

Fig. 4. AES, summer 1974. Ridges per 100 km ice cover; circled numbers identify areas profiled by Hibler et al (1974).

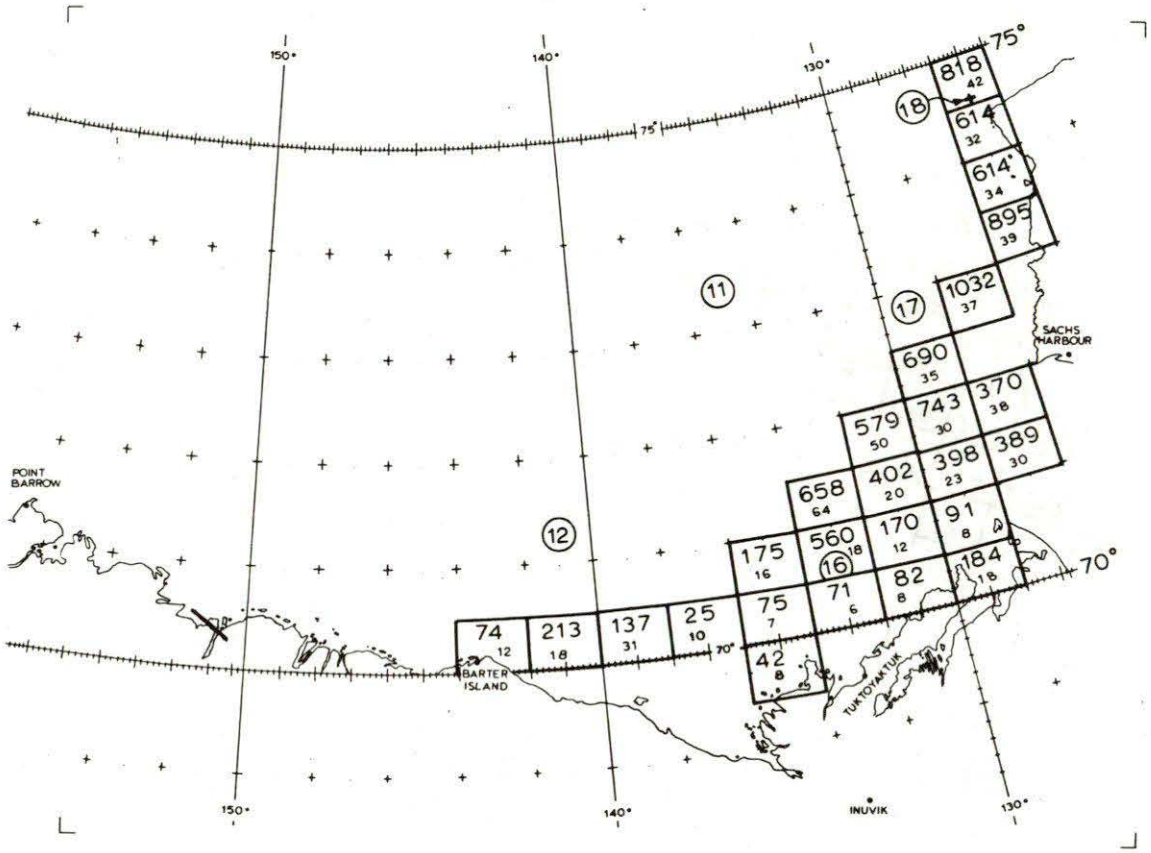

Fig. 5. AES, summer 1974. Ridges per 100 km of profiling track.

In Fig. 7 the mean ridge height is plotted against the number of ridges per km of ice cover. The results for the northern group of grid divisions (north of 71° 30') appear to fit a linear positive correlation, and a large number of the southern divisions appear to lie on the same regression line. However, a group of seven southern divisions (J, N, R, S, T, V and Z) have anomalously large mean heights. These all lie in the southeastern Beaufort Sea in a region of low percentage ice cover, and this suggests a possible reason for the anomaly. The ice in this region is very broken and scattered, but in origin it is a mixture of broken-out fast ice and ice from the first and most heavily-ridged part of the shear zone. The very edge of the winter shear zone (Kovacs and Mellor, 1974) consists of a narrow band of exceptionally heavy ridging with a very large mean ridge height (Klimovitch, 1972). A mixture of two such ice types would have a moderate ridge frequency (the diluting effect of the smooth fast ice) coupled with an anomalously high mean ridge height (from the shear zone ice). Such ice conditions are therefore atypical of the Beaufort Sea in general.

Leaving the anomalous values aside, the correlation coefficient between $\bar{h}$ and N is 0.86, which is significant at the 0.1% level on an analysis of variance test. It is physically reasonable to expect the stresses which generate a high concentration of ridges to also generate ridges with a greater mean elevation. A linear regression of $\bar{h}$ (mean ridge height in meters) on N (number of ridges per km of ice cover) yields

$$\bar{h} = 0.0201N + 1.201. \qquad \ldots(2)$$

The standard error of estimate is 0.040 m, and in Fig. 7 the regression line has been drawn in together with control limits placed one standard error of estimate on either side. It is thus feasible to estimate $\bar{h}$ for summer ridges in the Beaufort Sea when given N, which itself can be measured by cheaper means than laser profiling (e.g. analysis of aerial photographs). From these present results the order of accuracy would not be great - an estimate would have a 95% probability of being within ±0.08 m of the value given by the regression line - but it is reasonable to hope that with further data the control limits can be narrowed. This will greatly ease the routine gathering of sea ice morphology data in the future.

2.5 Distribution of Ridge Heights

Table 2 is a complete record of the ridges that were counted in each grid division. It is clear that the manual technique of measuring heights from a chart record introduces a bias to the results since the overall totals for integral numbers of feet greatly exceed those for half-foot intervals. The graticule used to estimate the heights was ruled in feet and a gestalt bias creeps in whereby the eye tends to take the ridge to the nearest whole number of feet instead of ascribing it to a half-foot interval. If the bias is a constant factor it means that, say, the 4-foot height class, instead of consisting of ridges between 3.75 feet and 4.25 feet, actually consists of ridges between (3.75 - δ) feet and (4.25 + δ) feet, where δ is a small constant of magnitude about 0.05 feet. Similarly, the 4.5 foot

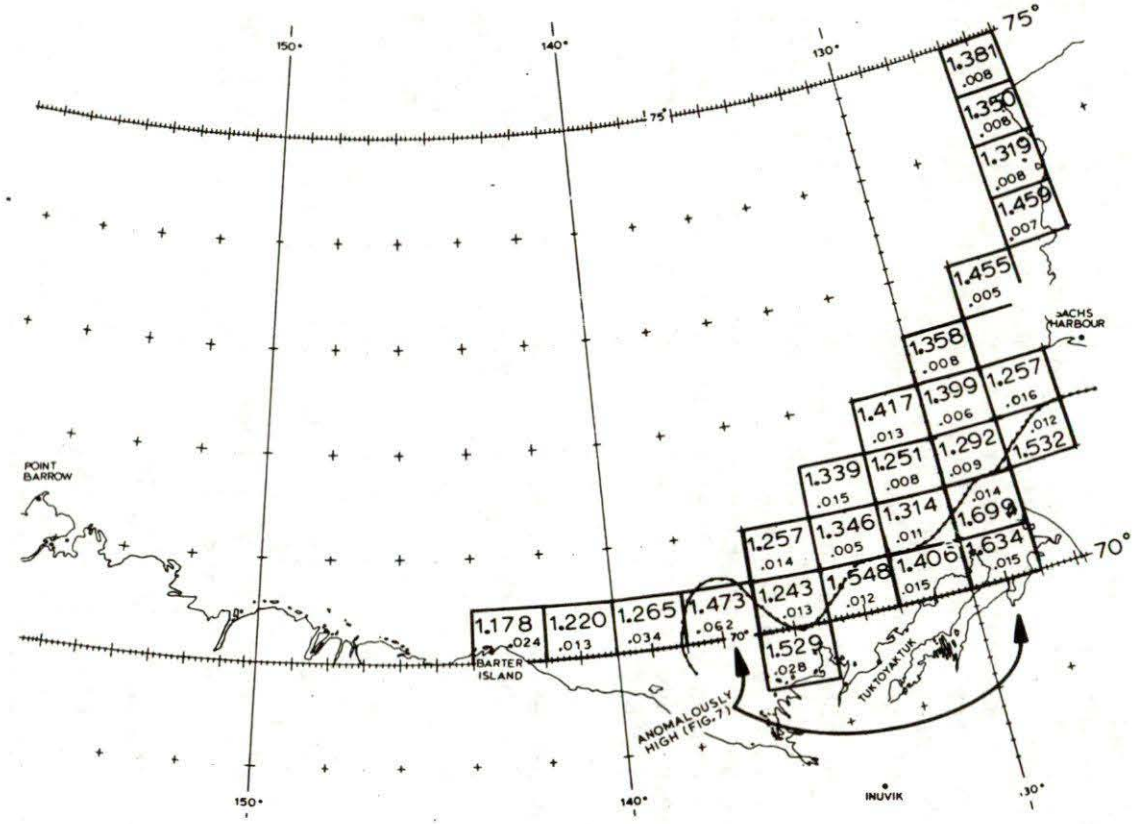

Fig. 6. AES, summer 1974. Mean ridge height in meters with standard error.

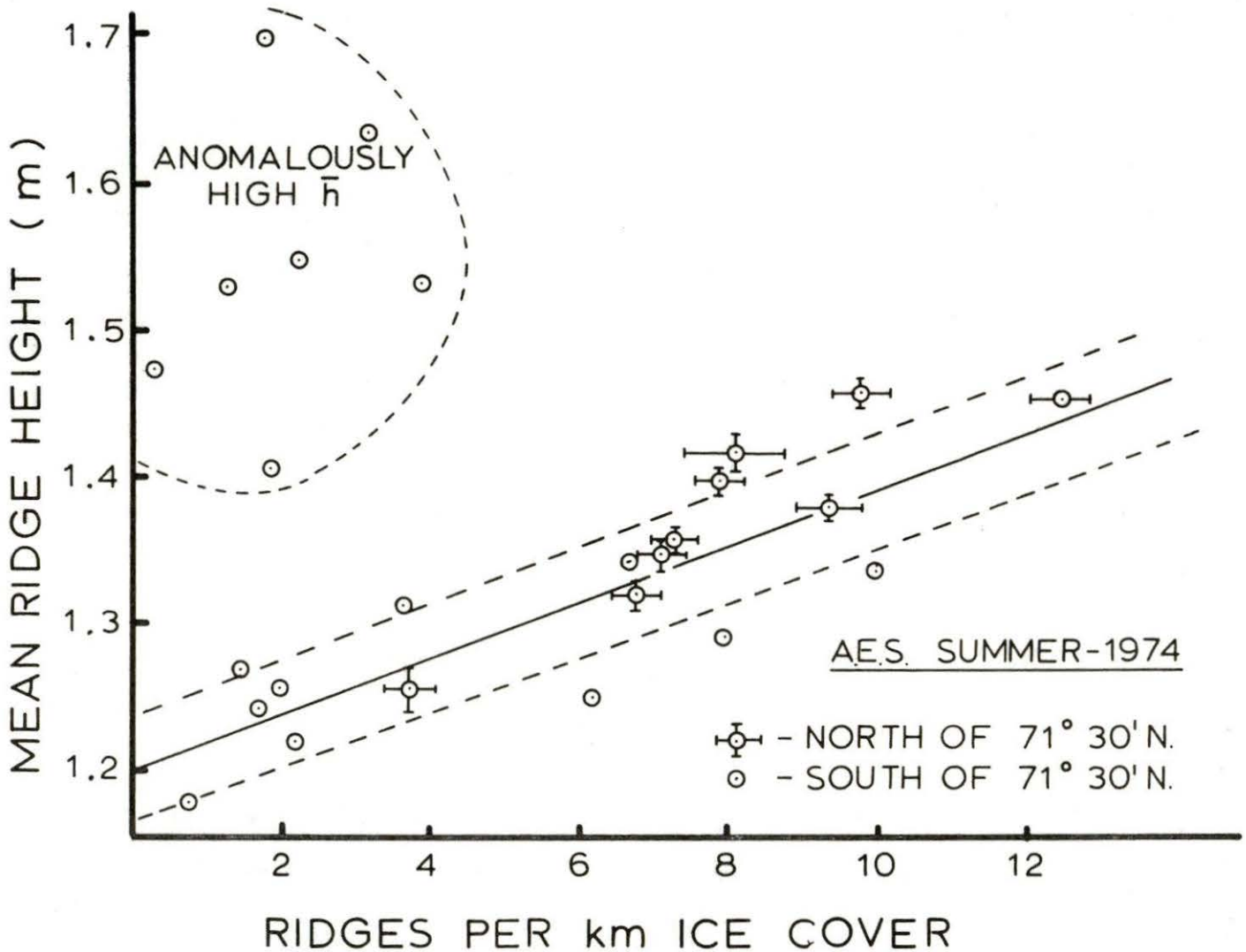

Fig. 7. Mean ridge height plotted against ridge frequency. Control limits are one standard deviation from regression line.

TABLE 2

Height, ft.

SW Corner of Grid	3	3½	4	4½	5	5½	6	6½	7	7½	8	8½	9	9½	10	10½	11	11½	12	12½	13	13½	14	14½	15	15½	16	16½	17	17½	18	18½	19	19½	20	20½	21	TOTAL
69½° N 136° W	8	4	3	4	3	1	1	1	1					1	1	1				1																		30
70° N 130° W	10	6	20	13	17	6	12	5	7	1	4	1	3	2		1			2																			110
70° N 132° W	22	15	24	5	15	2	14	1	6				1	1	1								1															108
70° N 134° W	44	18	22	7	20	3	10	5	8	1	6		4	1	5		1		3	1	1			1														161
70° N 136° W	50	22	22	15	9		3	2	2					3	1	1				1																		131
70° N 138° W	2	2							1				1																									6
70° N 140° W	3	8	5		1	1				1	1																											20
70° N 142° W	53	23	28	17	10	5	3	2	1	2			1	1				1																				147
70° N 144° W	17	8	5	4	3		1	1	2																													41
70½° N 130° W	14	11	21	15	21	2	13	1	4	1	3	2	5	1	2		1	1	2							1							1				1	123
70½° N 132° W	72	26	33	17	25	5	8	2	7		1			3	2	1	1						2															205
70½° N 134° W	294	129	151	68	101	26	52	17	37	6	15	7	10	4	3	4	1		6			1			1	1												934
70½° N 136° W	44	8	27	4	12	1	9	1	3		2	2																										113
71° N 128° W	32	20	32	10	22		10	4	12	3	5	1	4	2	2					1	1		1		1													163
71° N 130° W	120	49	46	14	23	8	19	3	4		5	3	1	3	3		1		1		1	1				1												306
71° N 132° W	127	55	79	25	47	8	20	7	9	2	8	1	2	2	1	2	2	1	2		1			1														402
71° N 134° W	41	12	20	4	10	1	4	1	4		4		1	1					1		2																	106
71½° N 128° W	40	10	16	6	10	2	5	3	1	1			1		2																							97
71½° N 130° W	196	72	94	35	61	19	31	12	24	9	16	4	14	1	6	2	1		1	1	1		2						1	1								604
71½° N 132° W	40	15	29	5	11	4	7	2	8	2	2	1	1	2			1		2										1									133
72° N 130° W	114	49	46	24	28	13	18	11	9	2	3	1	3		4	2	2	1	1	1					1			1										334
72½° N 128° W	260	78	135	35	70	26	44	18	33	8	24	9	16	3	15	1	5	3	6			1					1	1		2	1						1	796
73° N 126° W	177	59	89	24	46	15	30	5	23	4	20	5	7	4	7	3	8	1	2	2	3	1	2	2														539
73½° N 126° W	123	35	59	20	38	7	16	4	8	5	4		5	1	4	1	1		1														1					333
74° N 126° W	127	46	65	14	36	11	23	2	17	4	5	1	3	3		3	3	2	1								1											367
74½° N 126° W	119	54	68	19	29	17	22	11	16	4	11	1	6	3	2	2	1		1		1			1														388
TOTALS	2149	834	1139	404	668	183	375	121	247	56	139	39	89	42	61	24	29	10	32	8	11	4	8	5	3	3	2	2	2	3	1		2				2	6697

class consists of ridges only in the range $(4.25 + \delta)$ feet to $(4.75 - \delta)$ feet. If hand analysis is to be used it all, it is clearly necessary for a single analyst (in this case the author) to carry out all the measurements, so that the personal bias is fairly uniform throughout the data.

Without knowing the shape of the distribution in advance there is no valid way of redistributing the data even if a value for δ could be estimated. Therefore in attempting to compare the data with theoretical distributions we have two approaches: - the "whole-foot" and "half-foot" intervals can be treated as two separate populations; or the data from two adjacent intervals can be pooled, producing a histogram with foot-wide height intervals. The second approach is easier but has the disadvantage that the width of the interval becomes quite large in relation to the rapid decrease of ridge frequencies.

The only theoretical ridge height distribution proposed so far is that of Hibler et al (1972): -

$$P(h)\,dh = 2\lambda\bar{h}\;e^{\lambda h_0^2}\,e^{-\lambda h^2}\,dh \qquad \ldots(3)$$

where $P(h)$ is the probability density function for ridge height;

$\bar{h}$ is the mean ridge height, estimated from the data;
h_0 is the low-value height cutoff;
λ is a parameter which must be derived by iteration from the relationship: -

$$\exp\,(-\lambda h_0^2) = \bar{h}(\lambda\pi)^{\frac{1}{2}}\;\mathrm{erfc}\;(\lambda^{\frac{1}{2}}h_0) \qquad \ldots(4)$$

It should be noted that (3) is not an analytical expression, since $\bar{h}$ should be the mean of the distribution whereas in fact it is a sample mean. Hibler et al found that this distribution offered a good fit to large samples of ridge and keel data from various parts of the Arctic Basin.

Figure 8 shows the results of applying this distribution to our data. In Fig. 8(a) the overall totals are plotted in foot-wide height intervals (except for the 3 ft. height class which is kept separate) and the values predicted from (3) are shown in dotted lines. In this case h_0 was taken as 2.75 ft., i.e. δ was assumed to be zero, and the predictions were obtained by calculating.

$$\int_{h_1}^{h_2} P(h)\,dh \qquad \ldots(5)$$

where, for instance, the 3.5-4 ft. pooled class would have limits $h_1 = 3.25$ ft., $h_2 = 4.25$ ft. The fit is good only in the moderate height classes: we might expect a poor fit for the 3 ft. class, since these ridges are difficult to resolve against the background roughness, but in fact the fit is poorest in the highest classes. This is made more clear in Table 3(a) where experimental and theoretical values are compared directly. Here we have tested various values of δ, in each case taking h_0 as $(n + 1.25 + \delta)$ feet, h_1 as $(n + 0.25 + \delta)$ feet, and h_2 as $(n + 1.25 + \delta)$ feet. When $\delta = 0.1$ ft.,

the fit is generally improved up to a ridge height of 8 ft., but above this height all the predictions are similar and far too low. None of the predictions offer a significant likelihood of a ridge greater than 13 feet in height, whereas in fact the heights go up to 21 feet (for which theory predicts only 10^{-6} ridges!). It is apparent that the occurrence of high ridges in the coastal zone of the Beaufort Sea far exceeds the predictions of the Hibler theory. Referring to Table 2, we find that of the fourteen ridges observed with a height of 16 ft. or more, no less than twelve occur north of 71° 30', so that the area west of Banks Island is the chief source of these very high ridges. The highest free-floating ridge yet observed in the Arctic Ocean, with an elevation of 12.8 m (39 ft.), occurred slightly west of this area, at 74°N, 130°W (Kovacs et al, 1973).

In Figures 8(b) and (c) we consider the whole-foot and half-foot classes respectively as separate populations; in evaluating the theoretical distribution the integral in (5) is carried over a one-foot interval centred on the height class in question. Again we find a very poor fit with theory for the higher ridges. The objective may be raised that the overall ridge counts include ice from different areas with widely varying characteristics, so that a theory which holds true for a homogeneous profile may not hold true for the sum of many profiles. To test this, Figures 8(d) and (e) compare theory and experiment for the two-grid divisions with the highest ridge counts. Again the fit is poor, and in Table 3(b) we find that introducing various values for δ makes very little difference to the predictions for high ridges in the case of grid division E. A second possible objection is that our estimates of $\bar{h}$ are too low; in calculating $\bar{h}$ we consider each class as centred on its mean height value. For instance all ridges in the 4 ft. class are taken as being 4 ft. high, whereas in fact there are a greater number between 3.75 and 4 feet than between 4 and 4.25 feet. However, the effect of reducing $\bar{h}$ while keeping other parameters unchanged is to increase λ, and from (3) this can be seen to produce an even more rapid fall-off in ridge frequency with increasing height. The theoretical predictions will thus become even worse at the high end of the distribution.

Hibler et al derived their distribution by making two assumptions: - first, that all ridges are similar in geometrical cross-section (e.g. if the cross-section is idealized as an isosceles triangle, the angle of the triangle will be the same for all ridges); second, that all possible ridge height arrangements that yield the same net deformation of the ice cover are equally likely. The second assumption allows variational techniques to be used, as in statistical mechanics, to derive the ridge height distribution; of the ensemble of all possible icefields with a given quantity of deformed ice, one ridge height distribution can be shown to occur in the maximum number of possible ways, and this is the distribution that will be found in nature. Now Hibler's first assumption can be questioned because the slope angles of ridges are in fact quite variable, averaging about 19° for multi-year ridges (Kovacs et al, 1973) and 24° for first-year ridges (Kovacs, 1972). Let us suppose that ridges tend towards the same mean angle regardless of height, but that the angles are

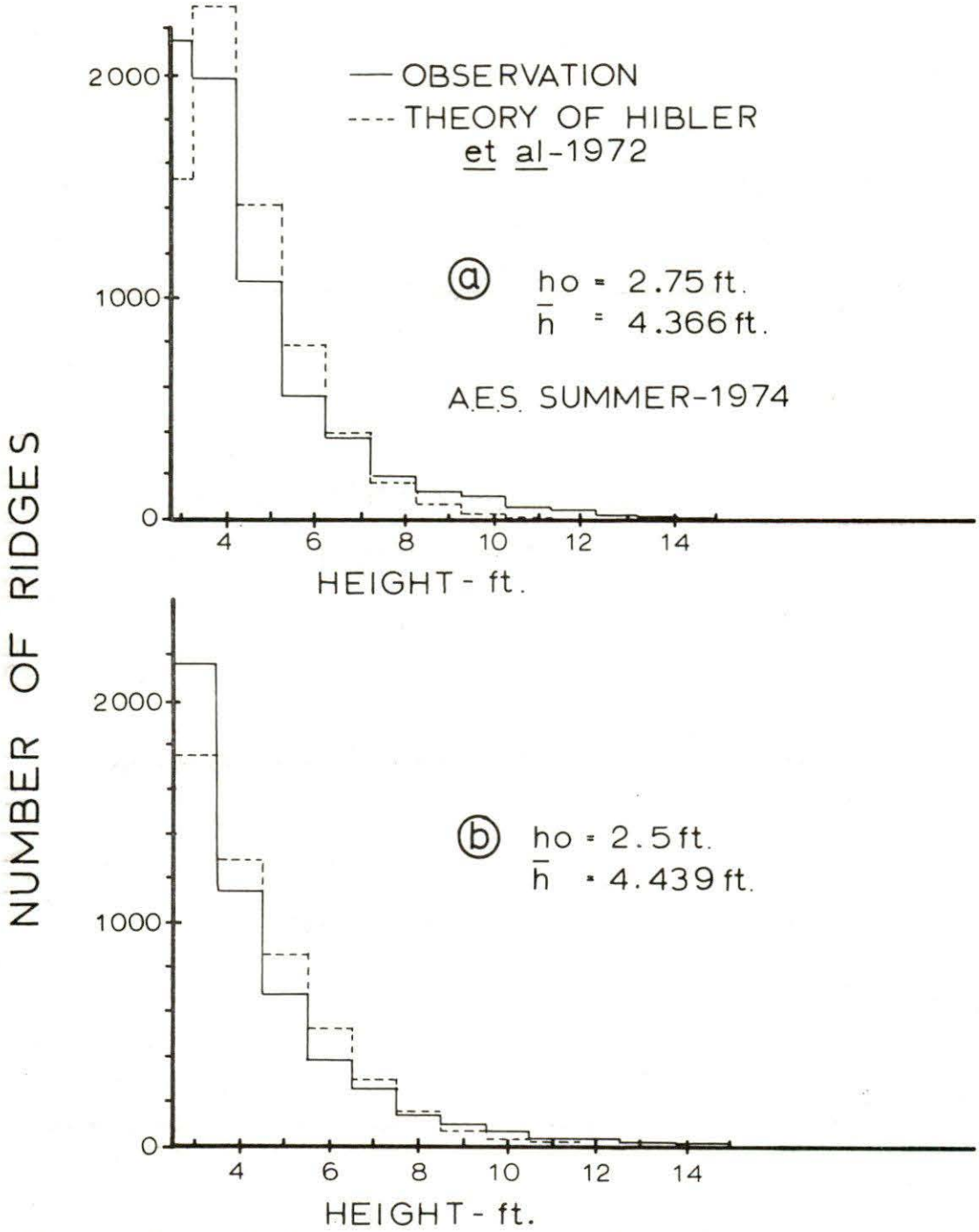

Fig. 8. Theoretical and observed ridge height distributions. (a) Overall results, summer 1974. (b) Results for height classes centred on whole numbers of feet.

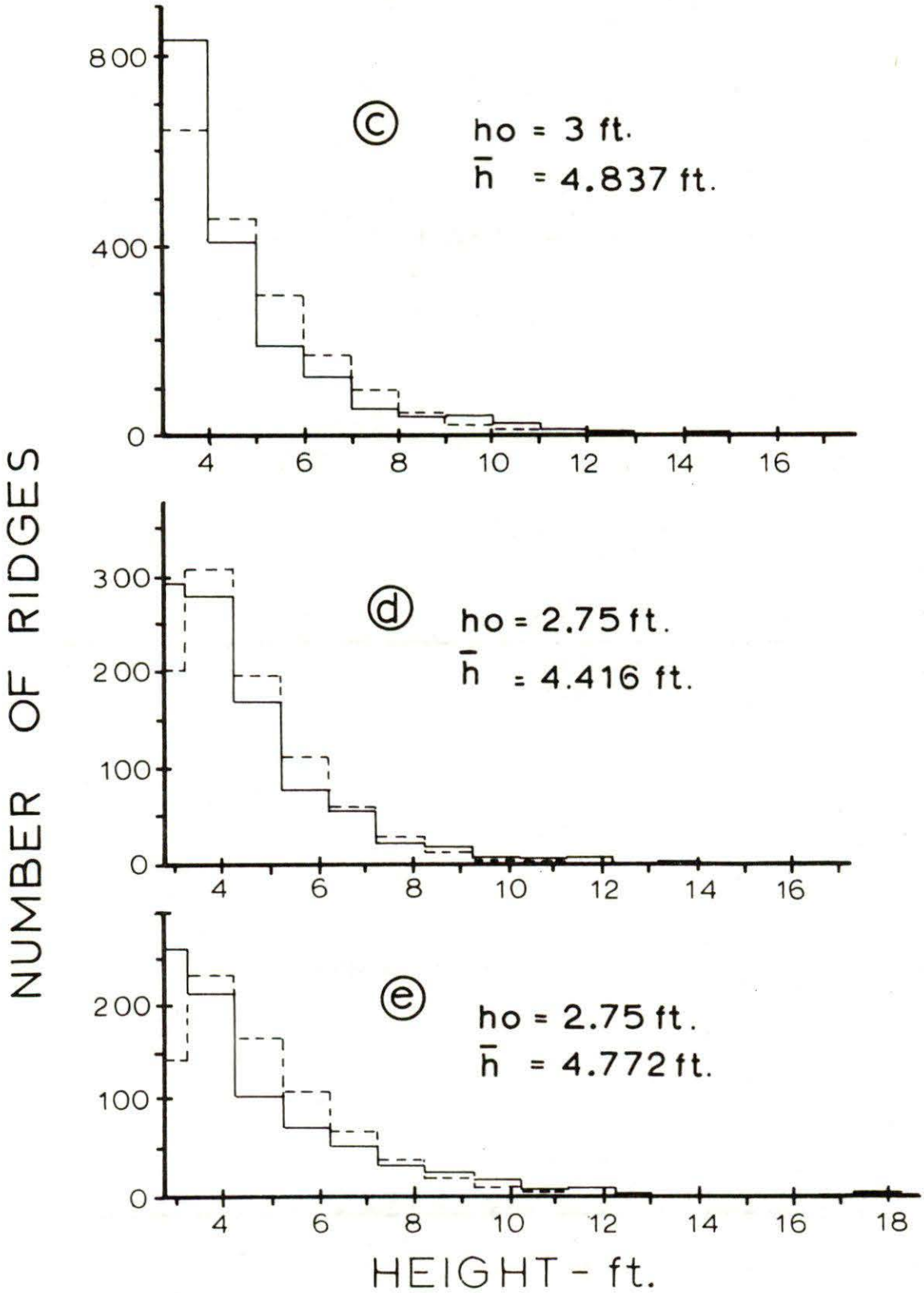

Fig. 8. Theoretical and observed ridge height distributions. (c) "Half-foot" categories. (d) Grid division P. (e) Gride division E.

TABLE 3a

Overall data for comparison of observed ridge counts with theory of Hibler *et al* (1972), with various values for bias factor δ.

Category ft	Observed	Theory δ = 0	δ = 0.05	δ = 0.1	δ = 0.15
3	2149	1532	1713	1896	1992
3.5-4	1973	2297	2134	2009	1855
4.5-5	1072	1417	1347	1286	1223
-6	558	780	764	743	734
-7	368	383	389	388	400
-8	195	168	178	183	199
-9	128	66	73	78	90
-10	103	23	27	30	37
-11	53	7	9	10	14
-12	42	2	3	3	5
-13	19	0.5	0.7	0.9	1
-14	12				
-15	8				
-16	5				
-17	4				
-18	4				
-19	2				
-20	0				
-21	2	$\simeq 10^{-7}$	$\simeq 10^{-6}$	$\simeq 10^{-6}$	$\simeq 10^{-6}$

TABLE 3b

Grid division E - SW corner 72° 30' N, 128° W

Category	Observed	Theory δ = 0	δ = 0.05	δ = 0.1	δ = 0.15
3	260	143	157	176	184
3.5-4	213	233	215	205	188
4.5-5	105	166	156	150	141
-6	70	110	105	103	99
-7	51	67	66	65	65
-8	32	38	39	39	40
-9	25	20	21	21	23
-10	18	9	10	11	13
-11	6	4	5	5	6
-12	9	2	2	2	3
-13	0	1	1	1	1
-14	1	10^{-1}	10^{-1}	10^{-1}	1
-15	0	10^{-2}	10^{-2}	10^{-1}	10^{-1}
-16	1	10^{-2}	10^{-2}	10^{-2}	10^{-2}
-17	1	10^{-3}	10^{-2}	10^{-2}	10^{-2}
-18	3	10^{-3}	10^{-3}	10^{-3}	10^{-3}
-19	0	10^{-4}	10^{-4}	10^{-4}	10^{-3}
-20	0	10^{-4}	10^{-4}	10^{-4}	10^{-4}
-21	1	10^{-5}	10^{-5}	10^{-4}	10^{-4}

distributed narrowly about this mean. The variational technique is still approximately valid, yielding the same distribution as before. But our new assumption will then cause this distribution to become flattened out. In other words, a given height class will spill its shallower ridges down into lower height classes and its steeper ridges up into higher classes. Since the distribution is monotonically decreasing, the result will be that the very highest classes receive more ridges from the lower classes than they lose to them. This explains the greater prevalence of very high ridges combined with a generally good fit to Hibler's distribution in the more moderate size classes. Thus distribution (3) cannot be used as a prediction system for high ridges.

3. RESULTS OF DND FLIGHTS, APRIL 1975

3.1 Technique

Two flights over the Beaufort Sea were made in April 1975 by a Canadair Argus aircraft of Maritime Proving and Evaluation Unit, CFB Summerside, PEI. Both flights began and ended at Inuvik. The first, on April 20th, followed the 135th meridian up to 76° 30'N and then ran westward as far as the AIDJEX camp at about 145°W, returning by the same route. The second, on April 26th, followed the same route northwards but returned along the 139th meridian and carried out an inshore survey before returning to Inuvik. Laser profiles were obtained throughout the first flight using a Geodolite profilometer, but this failed to operate during the second flight. In addition, side-looking airborne radar (SLAR) imagery was taken along the flight lines and in low level passes over the AIDJEX camp in support of a separate project carried out by R.O. Ramseier. Figure 9 shows the track of the laser profiling flight of April 20.

The laser terrain profile was recorded in analogue form on two magnetic tape systems - a 4-track recorder and a 14-track FM recorder - and the output of the profilometer was also monitored on an oscilloscope. This system permits a full quantitative analysis of the data to be carried out. The first step was digitization of the record on a 14-bit analogue-to-digital converter at 240 Hz using a 0 - 120 Hz low pass analogue filter to remove noise down to the Nyquist frequency. A high digitization rate (corresponding to 3 points per meter of profile) was necessary to resolve properly the structure of each ridge, especially across the peak so that the true height is recorded. The second step is removal of aircraft altitude variation, noise spikes and 360° phase shifts (where the profilometer trace returns to zero at the beginning of a new 100 ft. interval). This is best done using a computer technique developed at the Defence Research Establishment, Ottawa (Brochu and Lowry, 1975; Lowry and Brochu, 1975). The profile is displayed in sections of approximately 2 km on an interactive terminal, where spikes and phase shifts are removed manually. The operator then draws in a profile of aircraft motion by joining adjacent minima with straight line sections. The piecewise straight line profile is filtered to generate a smooth curve of aircraft motion, which is subtracted from the raw profile. The "clean" profile of pure terrain topography is returned to store and is then ready for computer analysis of ridge height and spacing distributions.

. 23

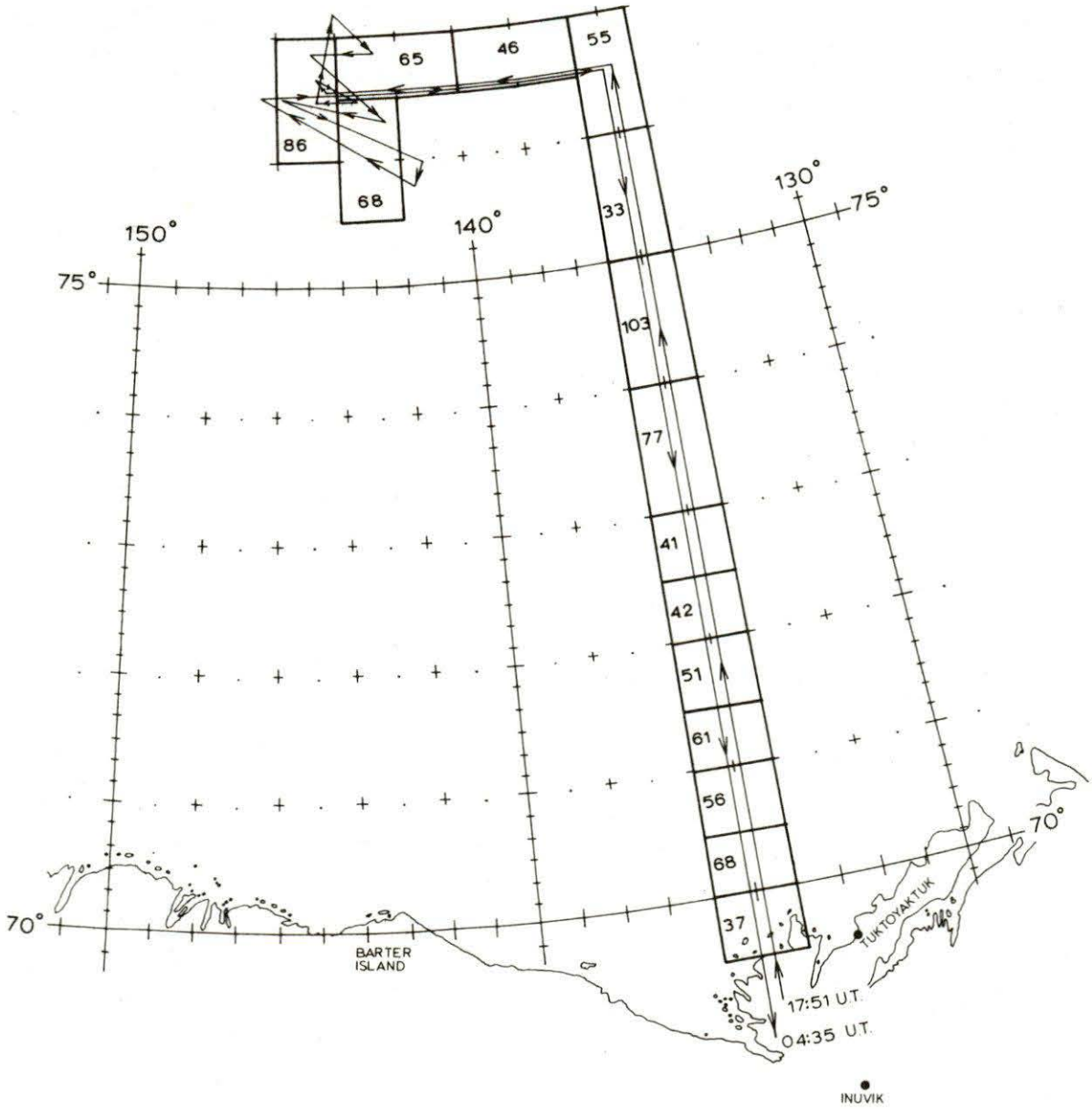

Fig. 9. Track of DND flight, 20 April 1975; grid divisions used for analysis of laser profiles; number of km of profile analyzed in each division.

3.2 Results of Laser Profiles

The area covered by the laser profile was analyzed in terms of a grid system similar to that used for the AES profiles. Figure 9 shows the arrangement of grid divisions; up to 73°N the size is 0° 30' of latitude by 2° of longitude, while further north where conditions change more slowly a coarser grid of 1° by 2° or 0° 30' by 4° is used. Figure 9 also shows the number of km of record analyzed in each division; the total track length treated was 889 km. The Argus is equipped with an inertial navigation system and position fixing on the laser record was of similar accuracy to the AES profiles.

Ridge heights were ascribed to categories of width 1.28 feet (0.39 m), corresponding to the scale graticule on the chart recorder. The noise level on the record was higher than for the AES records, and it was found that reliable ridge counts could be made only above a cut-off of 3 scale divisions (3.84 feet, 1.17 m). Assuming absence of bias in the analysis, the lowest height category therefore contains ridges with a minimum height of $2\frac{1}{2}$ divisions (3.2 feet, 0.98 m) and this is then h_0 as defined in (3). The higher cut-off means that ridge frequencies can be compared directly with the AES results only if the 3 ft. category in the AES data is ignored. Under these circumstances the AES cut-off is 3.25 feet (assuming $\delta = 0$), or 0.99 m, so the two sets of data are directly comparable, with almost identical h_0 values of approximately one meter.

Figure 10 shows the mean ridge frequency in each grid division expressed as ridges per 100 km of track with a standard error as defined in (1). Except in the vicinity of the wide lead at the edge of the shorefast ice (see Section 3.3) the ice cover was virtually 100%, broken only by narrow leads, and so the ridge frequency is also per 100 km ice cover. In the south the ridge frequency is low, corresponding to the fast ice zone (to 70°N) and the shear zone, which does not appear to be heavily ridged at this longitude. Further north the ridge frequency appears to increase slowly with latitude, an effect which is demonstrated in Fig. 11.

In only three grid divisions is a direct comparison possible with the AES data, together with one area in the polar pack for which Hibler presents data. The comparison is given in Table 4.

There are no clear trends in these comparisons, mainly because the three southerly grid divisions are in the very variable coastal zone of the Beaufort Sea. The ice there in summer is a mixture of seasonal ice and broken-out fast ice, and in April consists of the outer fast ice zone and then the edge of the shear zone which has already begun to open up. Therefore we can draw few conclusions except to note the low ridge frequency in April. The Hibler station shows a general constancy of ridge frequency except for an anomalously high value in March 1971. We note also from Fig. 11 a general clustering of frequencies in the polar pack at 1.5 to 2.1 per km except for a single high value of 3.1. Those familiar with the polar pack in the Beaufort Gyre (e.g. Herbert, 1970) report occasional large fields of pressured ice, sometimes 30 km in diameter, with very heavy

TABLE 4

Grid Division	Coordinates of S.W. Corner	Summer 1974 h_0 = 0.98 m			April 1975 h_0 = 0.99 m	
		Ridges per 100 km			Ridges per 100 km	
		ice cover	total track	$\bar{h}$ m	total track	$\bar{h}$ m
Z	69° 30'N, 136°W	92±20	31±7	1.75	22±8	1.32
U	70° 00'N, 136°W	105±12	46±5	1.44	81±11	1.61
Q	70° 30'N, 136°W	118±14	107±13	1.48	43±9	1.46
11 (h_0= 1.22m)	73° 00'N, 136°W	Jan '71 120 Mar '71 540 Mar '72 160 Feb '73 140			113±12	1.67

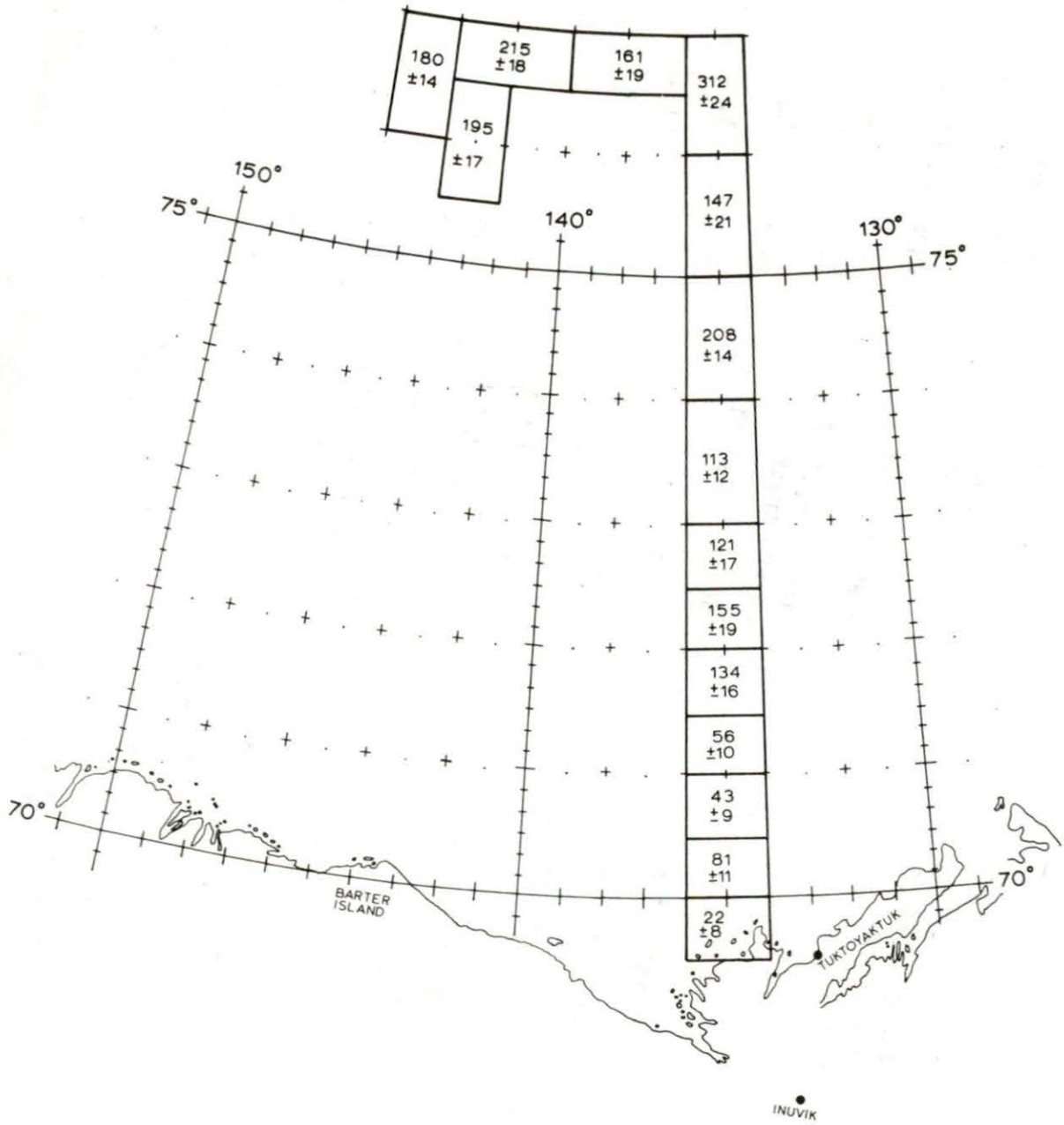

Fig. 10. DND April 1975. Ridges per 100 km profiling track.

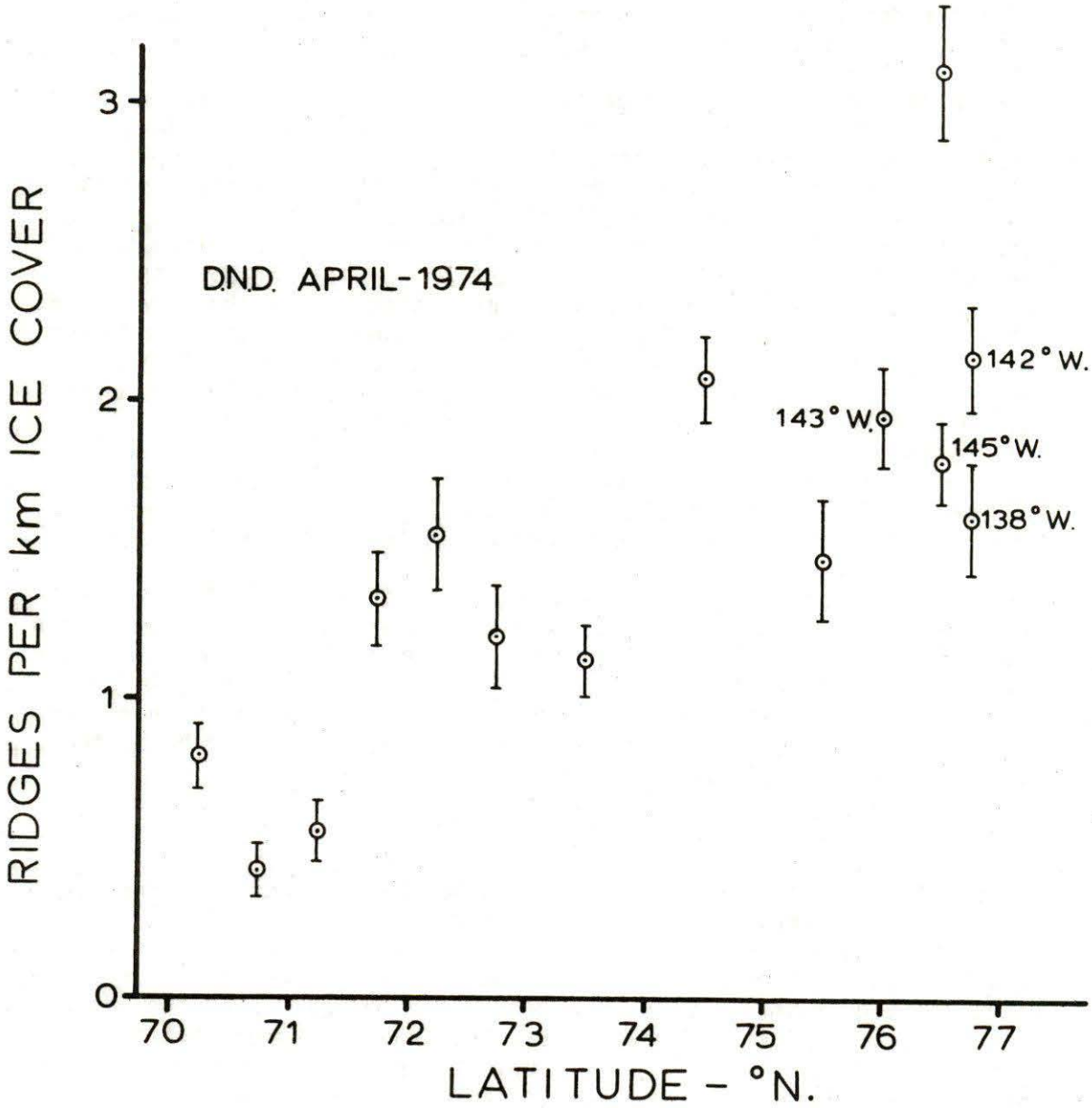

Fig. 11. Variation of ridge frequency with latitude. Longitude 135°W unless otherwise stated.

ridging. These are thought to be the result of pressuring of a large refrozen polynya. Such a field would give an anomalously high ridge frequency to the area in question, so we suggest that for winter ice in the Beaufort Sea Gyre the range 1.5 to 2.1 per km represents the normal ridge frequency. This is very much lower than the summer values found in the shear zone off Banks Island.

Figure 12 shows the mean ridge height in meters relative to the 0.99 m cut-off, together with the error. If we plot mean ridge height against ridge frequency we obtain Fig. 13 which is not a simple straight line as in Fig. 7. Three distinct regions can be distinguished: - the area south of 71° 30'N, incorporating the shear zone and outer fast ice, which has a low ridge frequency and a low mean height; the polar pack as far north as 75° 30' at 136° W, with a moderate ridge frequency and a large mean height; and the area north of 75° 30' and west to 146°W, which has a lower mean height and high ridge frequency. The last-named area corresponds roughly to the centre of the Beaufort Gyre, which has been located by Coachman (1969) at 80°N 140°W. The track at 136°W corresponds to the eastern part of the Beaufort Gyre, with a southward mean ice drift. Each region within itself shows a positive linear correlation between frequency and mean height, but the simple relationship found in the summer for the coastal Beaufort Sea does not occur in the winter polar pack.

The overall ridge height distribution is again quite different from the predictions of Hibler. Figure 14 compares theory and observation, and once again the observed frequency of high ridges is much greater than the prediction. In Section 4 we shall show that there is a remarkable agreement between the observed occurrences of high ridges in the AES and DND data, and that this can be used as the basis for an empirical prediction of extreme ridge heights.

3.3 Open Leads

During the flight of April 26th the author kept a count of open leads from the nose bubble of the aircraft during a 5½- hour flight. Only leads which passed directly under the aircraft's flight track were counted, and an "open" lead was defined as one possessing a continuous strip of open water or of very recently formed ice. From the air open water appeared black and new ice various shades of grey, getting lighter as the ice grew thicker. Only the black of open water or the very dark grey of ice only a day or two old were counted. Leads seemed to fall into two classes: - new leads, which were narrow cracks with clean edges snaking across the icefield and cutting level ice and pressure ridges alike; and old, wide leads which showed signs of frequent opening and closing and which were usually frozen over with thick ice except for a narrow active portion. As the aircraft flew south and entered the shear zone, the frequency of leads increased dramatically and the open leads themselves were wider, indicating a divergence in the stress on the pack. Finally a very wide lead (of estimated width 2 km) was crossed, marking the boundary of the shorefast ice. The outer part of the shorefast ice showed occasional cracks, indicating the earliest stages of break-up, but the inner zone was a continuous sheet.

. 29

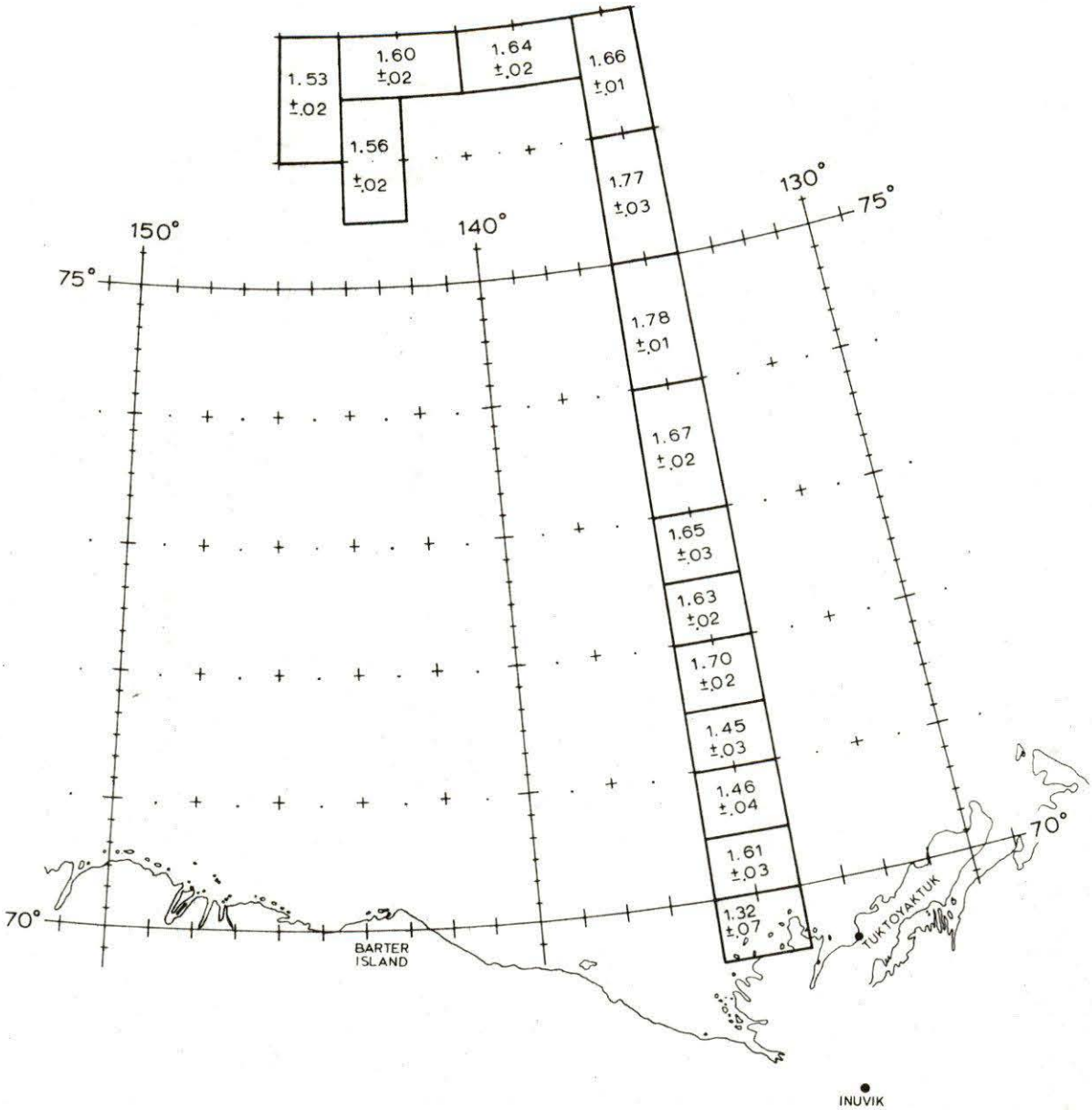

Fig. 12. DND April 1975. Mean ridge height in meters, relative to 0.99 m cutoff.

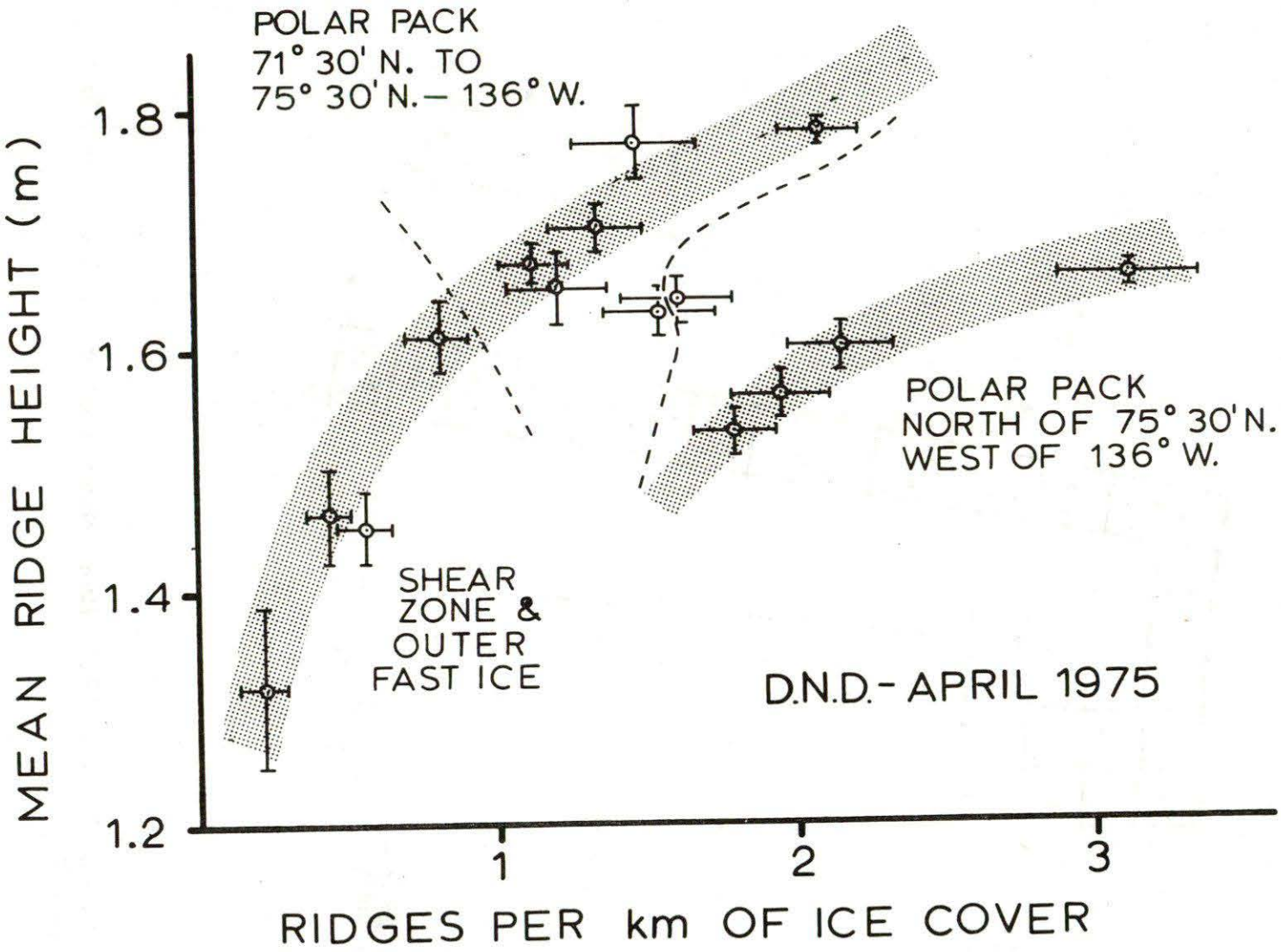

Fig. 13. Mean ridge height plotted against ridge frequency.

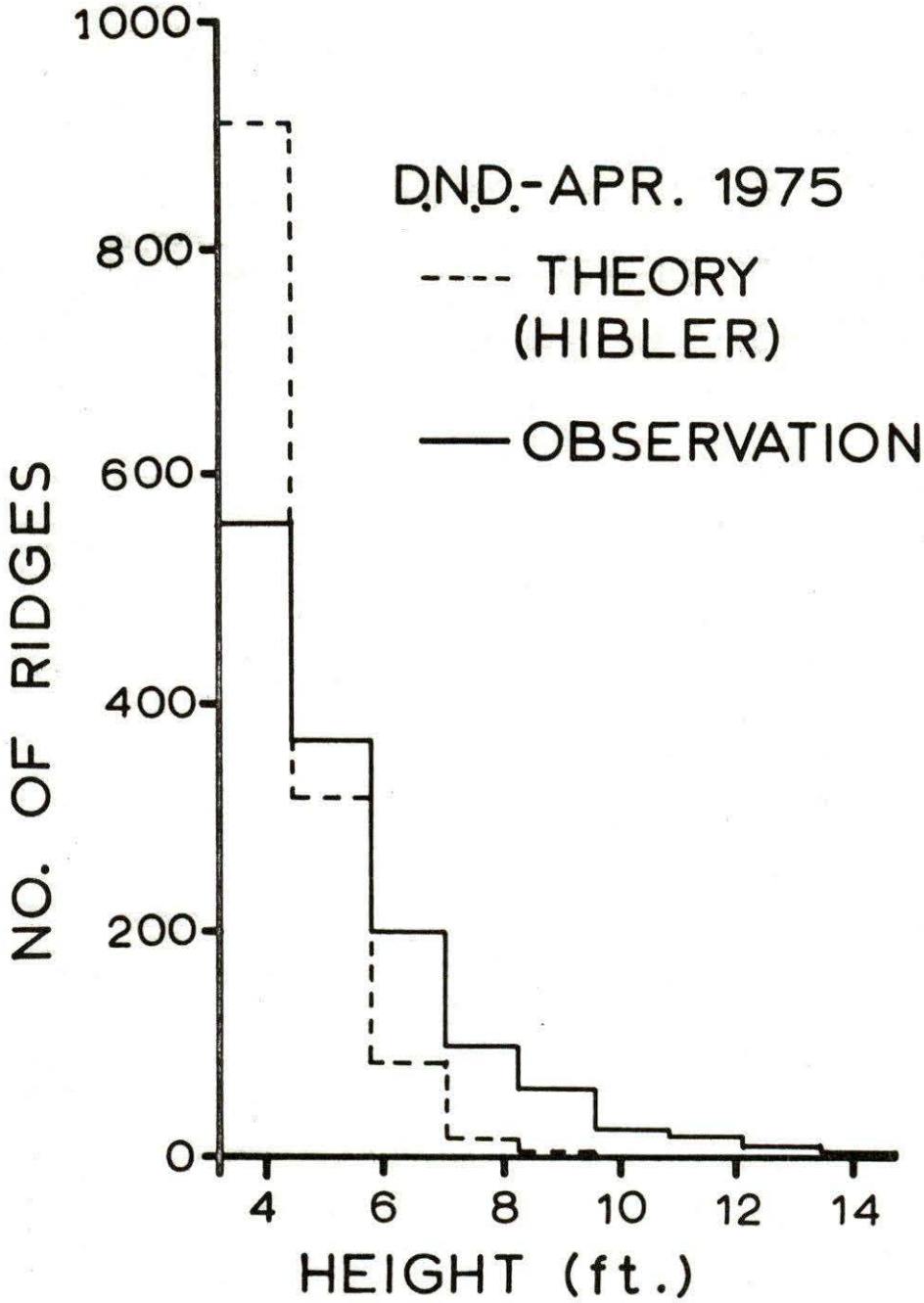

Fig. 14. Theoretical and observed ridge height distributions.

Figure 15 shows the track of the aircraft. After reaching Herschel Island the aircraft flew a pattern over Mackenzie Bay and eastwards to Cape Dalhousie. The wide lead was crossed several times and its path could be traced; it followed the approximate line of the 18-20 m depth contour, in agreement with the observations of Stringer (1974) for the north Alaskan coast. Figure 15 also shows the results of lead counts during successive 5-minute periods. Each of these counts was converted into a lead frequency per km using ground speed information from the aircraft flight log, and the results are shown in Fig. 16. It can be seen that a low lead frequency in the central polar pack gives way quite suddenly to a high frequency in the seasonal zone. It appears that the moving pack in the seasonal zone was beginning to open out and retreat prior to the spring break-up of ice in the fast ice zone. The data in Figure 16 can be summarized by the following mean values, which are compared with data obtained by Wittman (Weeks et al, 1971) in BIRDSEYE flights up to 1966: -

TABLE 5

DND April 1975	Mean Leads per km	Standard Deviation Leads per km
Polar pack	0.18	0.03
Shear zone	0.72	0.07
Outer fast ice	∿ 0.1	-
Inner fast ice	Nil	-
BIRDSEYE To 1966		
Shear zone (winter)	0.41 in openings > 30 m across 0.39 in openings < 30 m across	
Seasonal zone (summer)	0.18 in openings > 30 m across 0.72 in openings < 30 m across	

It can be seen that the lead frequency is about one order of magnitude less than the freqency of ridging.

4. PREDICTION OF MAXIMUM RIDGE HEIGHT

To assess the safety of sea bed operations on the shelf it is vitally important to know the maximum depth of keel that can be expected in a given linear stretch of track or a given area of icefield. In the absence of long underwater sonar profiles of the ice bottom to match the long laser profiles of the ice surface we are forced to approach the problem in two stages:

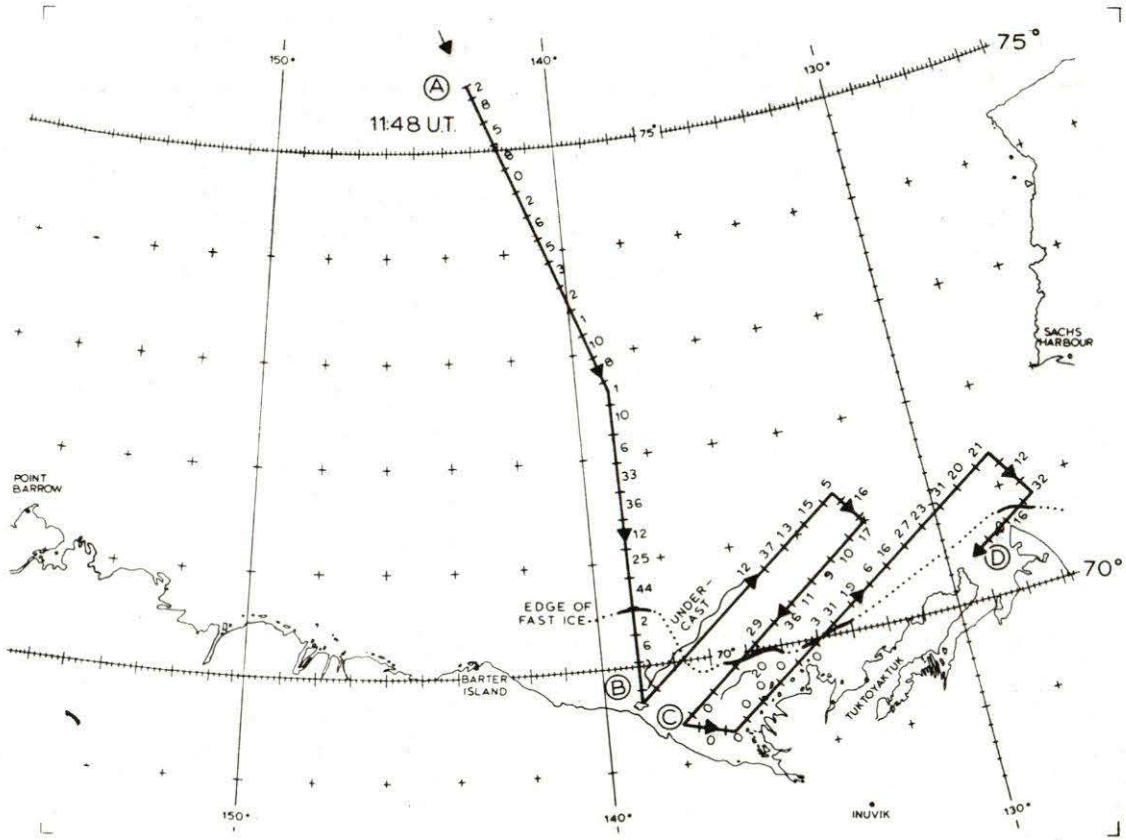

Fig. 15. Track of DND flight, 26 April 1975, and numbers of open leads counted in 5-min. periods.

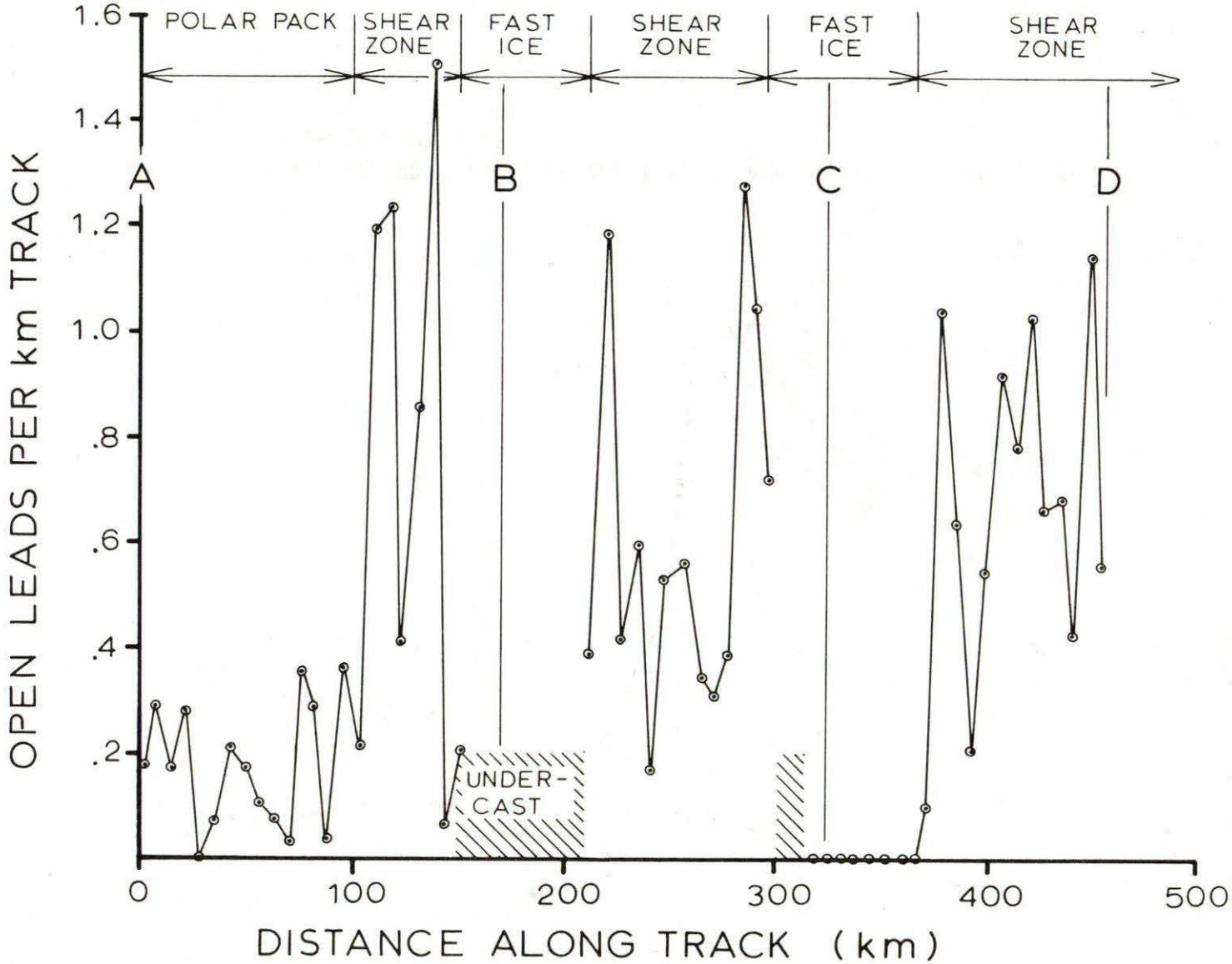

Fig. 16. Distribution of open leads, 26 April 1975.

1) Estimation of maximum ridge height along tracks or in areas;
2) Estimation of a conversion factor to obtain keel depth from ridge height.

Stage 2 is dealt with in Section 5 of this report.

We have shown that the distribution (3) is invalid for the prediction of high ridges in the area of interest. Fortunately our data appear to fit a simpler relationship, which can be used at least as a rule of thumb for this purpose. For the AES data Fig. 17a shows the pooled probability density per foot (i.e. number of ridges in two adjacent classes divided by total number counted) plotted on a log scale against the ridge height in feet. The results for different grid divisions all appear to lie on a single straight line; the divisions used each have enough ridges in them to test the relationship up to a height of 12 ft., and then the overall data permits the relationship to be tested up to 16 ft. The line of best fit has a gradient of about one decade per 5 ft. ridge height, and passes almost exactly through the origin. There is a slight positive deviation from the line for the lowest (4 and 5 ft.) classes, and there would be an even greater positive deviation for the 3 ft. class if it were plotted, so the relationship is valid only for higher ridges.

In Fig. 17b it is shown that the relationship holds for the DND data as well; in fact the pooled data from the AES and DND profiles fit an identical line. This is a remarkable result which suggests a general law governing ridge heights. To construct Fig. 17b the pooled AES data were adjusted to a cut-off of 0.98 m and compared with the pooled DND data which have a 0.99 m cut-off.

A linear regression of log P_f (where P_f is probability density per foot) on h_f (ridge height in feet) yields

$$\log_{10} P_f = -0.2121\ h_f + 0.372 \qquad \ldots(6)$$

with a standard error of estimate of 0.0572. The line of best fit together with control limits of two standard deviations are shown in Fig. 17b. We convert now to meters and express (6) as a decaying exponential. Thus if

$P(h)\ dh$ = probability that a ridge encountered at random will have a height in the range h to (h + dh) meters, given that its height is greater than one meter,

then (6) becomes

$$P(h)\ dh = 7.7269 \exp(-1.6026\ h)\ dh \qquad \ldots(7)$$

If we now make the tentative assumption that the relationship which holds over the range of observation continues to hold for higher ridges, we are in a position to estimate maximum ridge heights. Equation 7 can be used to predict the probability densities of very high ridges, and we can also define a probability of exceedance $P_c(h)$, or cumulative probability density function: -

$$P_c(h) = \int_h^\infty P(h)\ dh \qquad \ldots(8)$$

$P_c(h)$ is the probability that a ridge encountered at random will have a

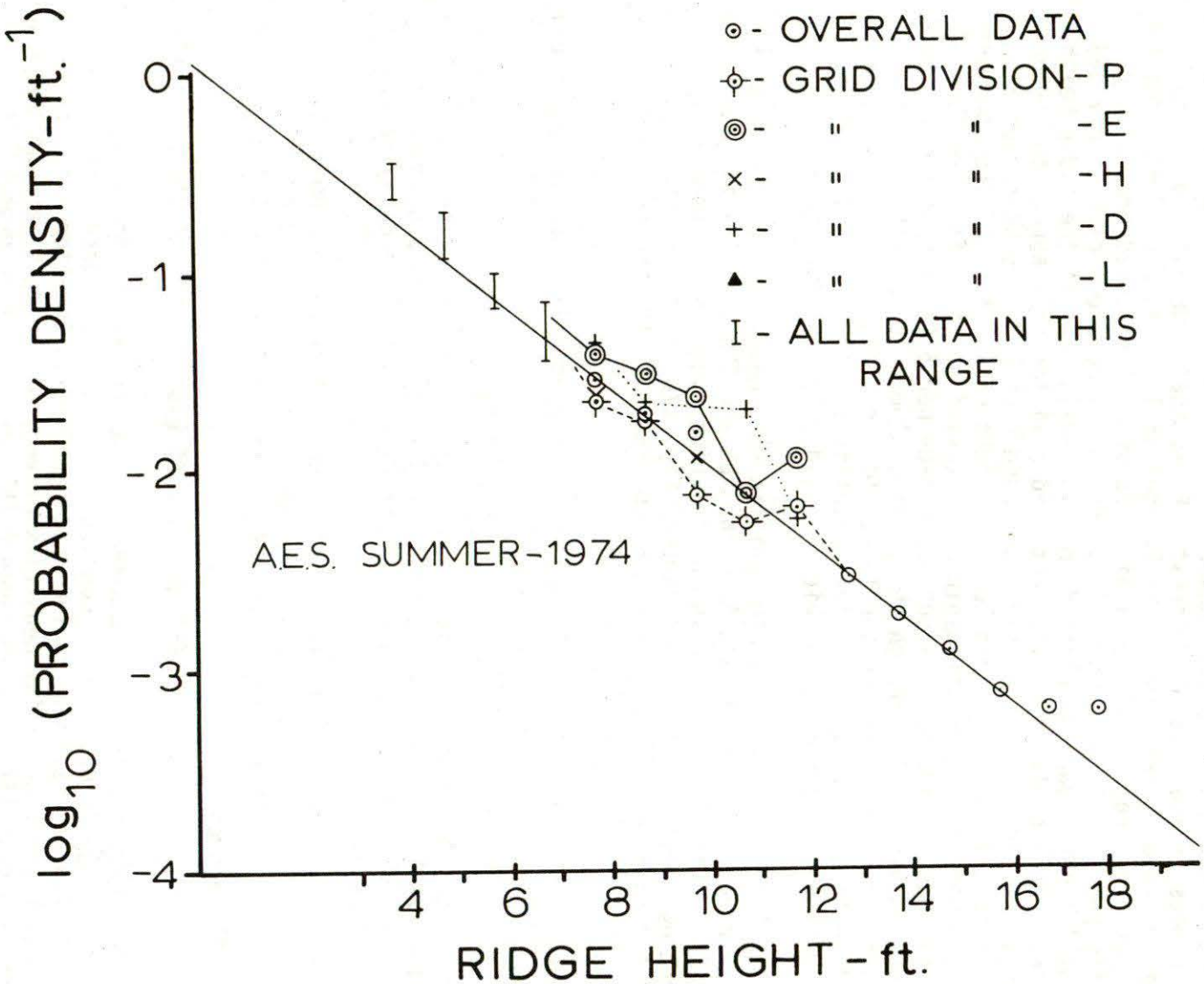

Fig. 17(a). AES summer 1974. Log-lin plot of observed ridge height distributions.

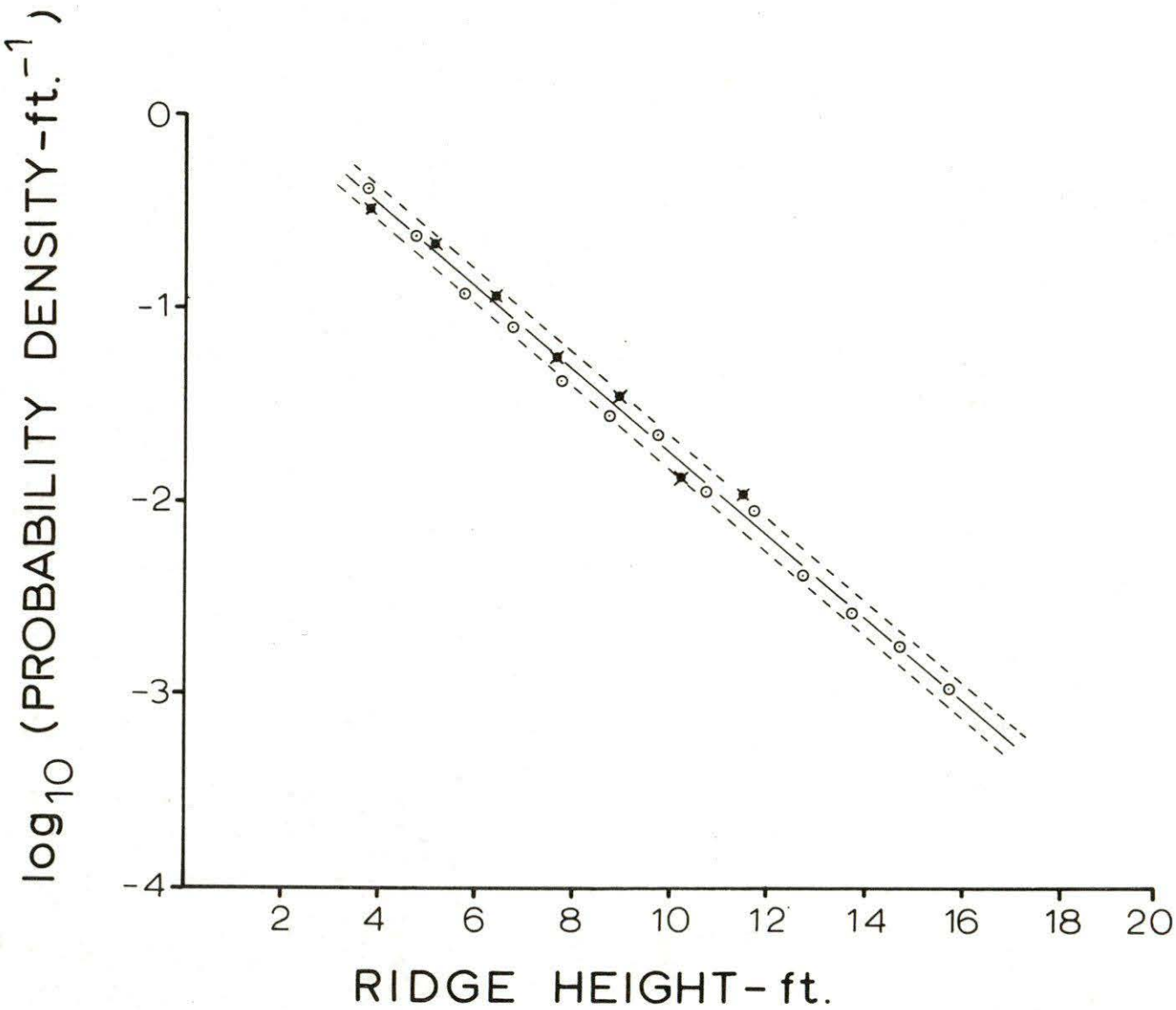

Fig. 17(b). Log-lin plot of observed ridge height distributions for AES data, summer 1974 (open circles) and DND data, April 1975 (closed circles). Control limits two standard deviations from regression line.

height of at least h meters. (7) and (8) give

$$P_c(h) = 0.6240\ P(h) \qquad \ldots(9)$$

Table 6 shows some probabilities for ridge heights up to 14 m. The standard error of estimate in Equation (6) is equivalent to an error of ±14% in P(h) and $P_c(h)$.

TABLE 6

Prediction Table for occurrence of high ridges

h Ridge height	P(h) Probability density	$P_c(h)$ Probability of exceedance
5 m	2.6×10^{-3} m^{-1}	1.6×10^{-3}
6 m	5.2×10^{-4} m^{-1}	3.2×10^{-4}
7 m	1.0×10^{-4} m^{-1}	6.5×10^{-5}
8 m	2.1×10^{-5} m^{-1}	1.3×10^{-5}
9 m	4.2×10^{-6} m^{-1}	2.6×10^{-6}
10 m	8.5×10^{-7} m^{-1}	5.3×10^{-7}
11 m	1.7×10^{-7} m^{-1}	1.1×10^{-7}
12 m	3.4×10^{-8} m^{-1}	2.1×10^{-8}
13 m	6.9×10^{-9} m^{-1}	4.3×10^{-9}
14 m	1.4×10^{-9} m^{-1}	8.7×10^{-10}

Use of the table is simplest if we wish to estimate maximum ridge height along a linear track. Suppose we consider a line of L km in a region where the mean ridge frequency is μ per km. Then we simply look up $(1/L\mu)$ in the exceedance table and this gives us the likely maximum ridge height along this line. For instance, a problem of great practical importance is to estimate a safe minimum depth for a sea bed operation (such as a wellhead or an instrument mooring) such that it will not be disturbed by a pressure ridge keel over a period of, say, a year. If the position of the operation is beyond the fast ice zone and within the moving ice of the Beaufort Gyre, the ice passing over this fixed point is equivalent to a track being profiled over stationary ice. In the seasonal ice zone the average winter ice drift is about 2.2 to 2.6 km/day (Coachman and Barnes, 1961), which is of the order of 10^3 km/year. Assuming heavy ridging of, say, 10 ridges/km, we have $L\mu = 10^4$ ridges. From the exceedance table we find that the likely maximum ridge height in such a sample is about 6.7 m (22 feet). Over ten years, with $L\mu = 10^5$, the likely maximum height encountered is 8.2 m (27 feet). On a more modest estimate of $L\mu = 10^3$, implying light ridging of 2 per km and a low mean annual drift of 500 km, we obtain a maximum ridge height of 5.3 m (17 feet). The final step, conversion to a maximum keel depth, will be considered in Section 5.

A rather more difficult problem is to estimate the maximum ridge height occurring at a given instant over a certain area of icefield. This may

arise when we ask such questions as, how many grounded ridges are there at a given moment in the outer fast ice zone? Questions concerning the possiblity of ice scour may also be cast in this form, although if we are asking whether ice scour could have taken place in a particular location over a certain historical period (an important question in the discussion of the true age of ice scours) we are asking a question of the linear type, concerning the number of ridges that have drifted over the point in the time allowed.

An approach to the area problem can be made using the concept of ridge density, R_0, developed by Mock et al (1972), this being the total length of ridging per unit area of icefield. The data of Mock et al from three areas of the Beaufort Sea give a roughly constant ratio of 1.6 between R_0 (estimated from aerial photographs) and ridge frequency μ. Now if $1/\mu$ is the mean spacing between ridges encountered on a straight line track, it is also the mean length that a ridge extends before being crossed by another ridge. Thus we can imagine the density R_0 in one square km being divided into ridge linkages each of length $1/\mu$; there will be $R_0\mu$ of these per sq. km. If it is valid to think of each ridge linkage as a separate ridge, then $R_0\mu$ ($=8/5\ \mu^2$) is the 'number of ridges per unit area', N_a. Then, to estimate maximum ridge height in an area A sq. km, we look up $1/AN_a$ in the exceedance table. As an example, let us estimate the maximum ridge height to be found at any given moment in the Beaufort Sea. The area of the Beaufort Sea continental shelf is 2×10^5 km^2, and of the whole Beaufort Sea (within a line from Prince Patrick Island to Point Barrow) $\simeq 4 \times 10^5$ km^2. Taking a value of about 8 ridges km^{-1}, we have $N_a = 10^2$ km^{-2}, and thus

$$1/AN_a \quad \begin{array}{ll} 5 \times 10^{-8} & \text{(shelf)} \\ 2.5 \times 10^{-8} & \text{(total).} \end{array}$$

From the exceedance table the likely maximum ridge height is about 11.5 m (38 feet) for the shelf and 11.9 m (39 feet) for the whole Beaufort Sea. The good agreement with the 12.8 m ridge found by Kovacs et al (1973) shows that this approach may have some quantitative validity. We must emphasize its speculative nature, however; a great deal more data is required before these prediction tables can be regarded as reliable.

5. MORPHOLOGY OF ICE KEELS

5.1 Conversion of Ridge Height to Keel Depth

No valid deterministic or even statistical means of converting ridge height to keel depth has been established. To do so we require long simultaneous profiles of top and bottom surfaces along approximately the same tracks, as may be obtained by a submarine acting in cooperation with an aircraft employing a laser. Estimates of the conversion factor are mainly averages based on a relatively small number of ridges that have been laboriously drilled through or profiled from the side using sonar. We do not even expect the conversion factor to be a constant, since the overall isostatic distribution of mass above and below sea level depends on the shape of the ridge, its age (i.e. snow and ice densities within it) and mode of formation.

This was recognized by Ackley et al (1974), who devised two theoretical models for keel depth conversion. The first was point isostatic (i.e. each point on a ridge generates a point directly below it on the keel), but took account of the variation of ice density with ridge thickness. The second allowed for the fact that the mass of a ridge is distributed over a larger area in the keel, and the conversion is done by a linear sawtooth filter which acts on the surface ridge profile. Thus the second model, while more realistic physically, does not generate a constant conversion factor.

Both models use an empirical relationship between the mean specific gravity ρ_i of an ice column and its freeboard f_i in meters: -

$$\rho_i = 0.974 - 0.194\, f_i \qquad f_i < 1.077$$
$$= 0.765 \qquad f_i \geqq 1.077 \qquad \ldots(10)$$

This is the mean of a large number of measurements on multi-year floes and ridges. For a ridge higher than 1.08 m, Equation (10) implies a ratio of 3.0:1 for draft:freeboard on a point isostatic model. The draft:freeboard ratio R is simply given by

$$R = \rho_i(\rho_W - \rho_i) \qquad \ldots(11)$$

where ρ_W, the specific gravity of displaced water, is taken by Ackley et al to be 1.0203. For level ice, with $f_i \ll 1.08$, the ratio is much higher than 3. The distributed model gives a lower R than the point isostatic for any idealized ridge shape, because the point on the keel directly beneath the ridge crest is generated by a convolution over a range of ridge freeboards which are all less than that of the crest. A 1975 Gulf Oil observational study in the coastal Beaufort Sea found close agreement with the point isostatic ratio for free-floating multi-year ridges. First-year ridges appear to have a higher ratio, however, and Kovacs (1972) found a mean value of 4.2:1.

The conversion of data from laser records is complicated by the fact that the laser measures ridge height above the level ice surface rather than ridge freeboard. If the freeboard of ambient level ice is f_0, a ridge of height h has a freeboard $f_0 + h$) and a correspondingly increased draft. There are now three ratios of interest: -

R (keel draft) : (ridge freeboard)

R_2 (keel draft) : (ridge height, given by $R_2 = R(f_0 + h)/h$ ...(12)

R_3 (keel depth below level ice bottom) : (ridge height), given by $R_3 = R(h + 2f_0 - t)/h$ ...(13)

where t is the level ice thickness and is related to f_0, according to Equation (10), by

$$t\,(0.974 - 0.194\, f_0) = (t - f_0)\,\rho_W \qquad \ldots(14)$$

R_2 is the ratio of importance in considerations of ice grounding and safe depths of water, while R_3 is of interest in considering the geometrical barrier offered by a keel to spreading oil; $R_3<R<R_2$. According to Maykut and Untersteiner (1969) the mean value of t in the Arctic Basin is 3.0 m in April and 2.7 m in September, and Koerner (1970) found a mean thickness of 2.8 m in multi-year floes over a year. These give values for f_0 of 0.317 m, 0.252 m, 0.272 m respectively, using equation (10).

To summarize, the draft/height ratio is greater than R by a factor which diminishes with increasing ridge height, and which is about 30% for a 1 m ridge. To offset this, the more realistic distributed isostatic model implies a lower value for R at a ridge crest. For simplicity, we shall take the draft/height ratio R_2 to be 3.0:1 for ice in the polar pack (which is mainly multi-year) and 4.0:1 for ice in the shear zone or offshore province (which is mainly first-year). Depth predictions will be made on this basis.

5.2 Maximum Keel Drafts

Table 7 is the result of converting Table 6 data into a keel draft prediction table using two possible values for R_2. We now have a probability density $P^k(h)$, which is the probability per meter that a randomly encountered keel will have a draft h meters; and a probability of exceedance $P_c^k(h)$, which is the probability that a randomly encountered keel will have a draft of at least h meters. These are related to P(h) and $P_c(h)$ by: -

$$P^k(h)\ dh = \frac{P(h/R_2)}{R_2}\ dh \qquad \ldots(15)$$

$$P_c^k(h) = 0.624\ R_2\ P_c(h) \qquad \ldots(16)$$

In Section 4 various ridge height maxima were estimated, which can now be converted to keel drafts. For ridges crossing a given point in the shear zone the 5.3 m figure for a year's maximum based on light ridging and slow drift becomes 21.2 m in draft; 6.7 m for a yearly maximum based on heavier ridging and faster drift becomes 26.8 m in draft; and 8.2 m for a ten-year maximum becomes 32.8 m. These estimates are all subject to the wide uncertainty in R_2, but we can compare them with various phenomena found on the Shelf.

First, 20 m is the normal maximum water depth for shorefast ice, corresponding to the maximum depth at which significant numbers of firmly grounded pressure ridges are found. A keel would have to be rather deeper than 20 m while freely floating in order to drive itself aground at that depth.

Ice scouring of the sea bed has been extensively mapped in recent years, both off Alaska (Reimnitz and Barnes, 1974) and in Mackenzie Bay (Pelletier and Shearer, 1972; Shearer and Blasco, 1975; Lewis, 1975). If is found that scouring is common between water depths of 10 m and 50 m, with a scour frequency of about 10 per km which shows a broad peak at around 30 m depth. About 50 m depth the frequency falls sharply, with no scours beyond 75 m. The scours in

TABLE 7

Prediction Table for Occurrence of Deep Keels

Keel Draft	Offshore Province $R_2 = 4.0$		Polar Pack Ice $R_2 = 3.0$	
m	Probability density m^{-1}	Probability of exceedance	Probability density m^{-1}	Probability of exceedance
20	6.4×10^{-4}	1.6×10^{-3}	5.9×10^{-5}	1.1×10^{-4}
22	2.9×10^{-4}	7.2×10^{-4}	2.0×10^{-5}	3.8×10^{-5}
24	1.3×10^{-4}	3.2×10^{-4}	7.0×10^{-6}	1.3×10^{-5}
26	5.8×10^{-5}	1.4×10^{-4}	2.4×10^{-6}	4.5×10^{-6}
28	2.6×10^{-5}	6.5×10^{-5}	8.2×10^{-7}	1.5×10^{-6}
30	1.2×10^{-5}	2.9×10^{-5}	2.8×10^{-7}	5.3×10^{-7}
32	5.2×10^{-6}	1.3×10^{-5}	9.7×10^{-8}	1.8×10^{-7}
34	2.3×10^{-6}	5.8×10^{-6}	3.3×10^{-8}	6.2×10^{-8}
36	1.1×10^{-6}	2.6×10^{-6}	1.1×10^{-8}	2.1×10^{-8}
38	4.7×10^{-7}	1.2×10^{-6}	3.9×10^{-9}	7.4×10^{-9}
40	2.1×10^{-7}	5.3×10^{-7}	1.4×10^{-9}	2.5×10^{-9}
42	9.5×10^{-8}	2.4×10^{-7}	4.6×10^{-10}	8.7×10^{-10}
44	4.3×10^{-8}	1.1×10^{-7}	1.6×10^{-10}	3.0×10^{-10}
46	1.9×10^{-8}	4.8×10^{-8}	5.5×10^{-11}	1.0×10^{-10}
48	8.6×10^{-9}	2.1×10^{-8}	1.9×10^{-11}	3.5×10^{-11}
50	3.8×10^{-9}	9.6×10^{-9}	6.5×10^{-12}	1.2×10^{-11}

deeper water are partially filled with sediments, suggesting that they are relics of a period when sea level was lower; the sedimentation rate is only about 1 m per 1000 years. The broad scour shapes made by ice island fragments can be distinguished from the parallel narrow tracks made by the deepest blocks of a single pressure ridge keel, and pressure ridge scours are found throughout the depth range. Using present sea level we can estimate the maximum depth at which scouring is common by supposing that a scour preserves its identity for approximately 1000 years, and that the criterion for "frequent scouring in a given area" is that a given point should enter the exceedance table at one scour per 1000 years. For 1000 years we have $(L\mu) \simeq 10^7$, but this should possibly be reduced by a factor of 2 to take account of the fact that ice drift is slower in the inner portion of the shear zone nearest the shorefast ice, since once a ridge has grounded it may hold up the motion of a large area of ice around it for a considerable period. Thus with $(1/L\mu)$ as 2×10^{-7} the exceedance table gives about 42 m as the likely maximum depth. At this depth every point on the bottom has the expectation of being struck at least once per 1000 years by a ridge, so scouring out to a depth of at least 40 m can be accounted for by pressure ridge grounding at present sea level.

During a submarine transit of about 1200 km in the Trans-Polar Drift Stream, Swithinbank (1972) found a maximum draft of 30 m. The ice in this area is mainly first-year, and assuming heavy ridging of 8 per km we have $L\mu \simeq 10^4$ and an expected maximum draft of 26.8 m, somewhat less than observed.

In summary, the figures for maximum ridge heights at any instant on the Beaufort Sea or Shelf - 11.5 and 11.9 m - convert to drafts of 46.0 and 47.6 m respectively. The entire Arctic Ocean ice cover has an area of 1.5×10^7 km^2, and we can use the ridge density model developed in Section 4 to estimate the maximum draft at any instant. We estimate the overall mean ridge frequency at between 3 and 5 per km, and we use a composite figure of 3.5 for R_2 on the assumption that the Arctic cover is 50% multi-year ice. These values yield estimated maxima of 45 m and 48 m respectively for the 3- and 5-ridge cases. The similarity of these estimates to those for the much smaller area of the Beaufort Sea is mainly due to the sensitivity of the keel prediction table to variations in R_2. The first conclusion is that since R_2 is not yet known to any accuracy the keel draft predictions must be regarded as very approximate. The second conclusion is that the coastal areas of the Arctic, such as the Beaufort Sea, are probably the site of the deepest keels in the Arctic Ocean, since they have a combination of high ridge frequences and high R_2 (on account of the preponderance of first-year ice). The deepest keel yet measured in the Arctic Ocean was in an unspecified location and had a draft of 47 m (Lyon, 1967).

5.3 Depth Fluctuations along a Solitary Keel

The effective geometrical depth which a keel presents to an approaching oil slick is not its mean depth, but the minimum depth relative to the level ice bottom in the keel linkage considered. Similarly,

when scouring occurs the first part of a keel to take the ground is that point on the crest which has a maximum draft. The jumbled block structure of a keel results in a random crest profile with significant fluctuations about the mean depth. An opportunity to study these arose when a sonar profile was obtained along a keel crest by an unmanned arctic research submersible (UARS) of the Applied Physics Laboratory, University of Washington (François and Nodland, 1972, 1973). The original sonar profile data were made available to the author by R.E. François.

The profile was taken on May 9, 1972, from ice island T-3 which was then very far north in the Beaufort Gyre at 84°N, 84°W. The ridge concerned was a shear ridge, estimated to be 6 to 8 years old, which lay in the sea ice of Colby Bay, an indent in the "coastline" of T-3. The remote-controlled UARS ran a star-shaped pattern at a depth of 46 m, and in one of its runs successfully profiled some 330 m of the ridge keel. Three sonar profiles were obtained simultaneously by narrow-beam (1°) transducers, one of which looked directly upwards while the other two looked sideways at 6° to the vertical. Figure 18(a) shows the output $y(x)$ of profiler 2 (vertical); profiler 1 looked to the left and thereby obtained a parallel profile offset laterally by 4.4 m, while profiler 3 failed to pick up the keel. The local draft of level ice (2.576 m) has been removed from Fig. 18(a) leaving only the relief of the keel.

It is apparent that the variance consists of a short-wavelength scale due to the block structure of the keel and a long-wavelength scale due either to a real variation in mean keel depth or, more likely, to a meander in the line of the keel so that the rectilinear track of the UARS did not remain directly beneath the crest. To estimate the fluctuations due to the block structure alone it is necessary to remove the long-wavelength variations. The profile was digitized at 0.325 m intervals, giving 1024 points (overall length 332.1 m), and a low-pass profile was generated using a 101-point running mean with reflections at both end points. Figure 18(b) shows the low-pass profile $y_0(x)$, whose depth varies from 0.321 m to 3.377 m. The greatest depth probably corresponds to the true mean keel depth, while all lesser depths refer to side slopes of the keel. It is thus a relatively shallow keel, with an overall draft of 5.95 m; the surface ridge has a height of about 1.7 m (François and Nodland, 1972).

We wish to estimate the minimum and maximum keel reliefs $y_{min}(\ell)$ and $y_{max}(\ell)$ in a given keel linkage ℓ. Ideally we would like a means of predicting such values for any ℓ and any mean depth $\bar{y}$. For a profile which is a Gaussian random function Cartwright and Longuet-Higgens (1956) showed that the elevations of the highest peak and lowest trough in a given linkage can be predicted in terms of the mean number of peaks per unit distance and a spectral width parameter derived from the power spectrum of the profile. The test for the Gaussian nature of this profile a series of local standard deviations $\sigma(y_0)$ was calculated for 0.5 m-wide categories of depth y_0. The deviation $[y(x) - y_0(x)]/\sigma(y_0)$ was then calculated for each value $y(x)$ with the results shown in Fig. 19. There is a clear departure

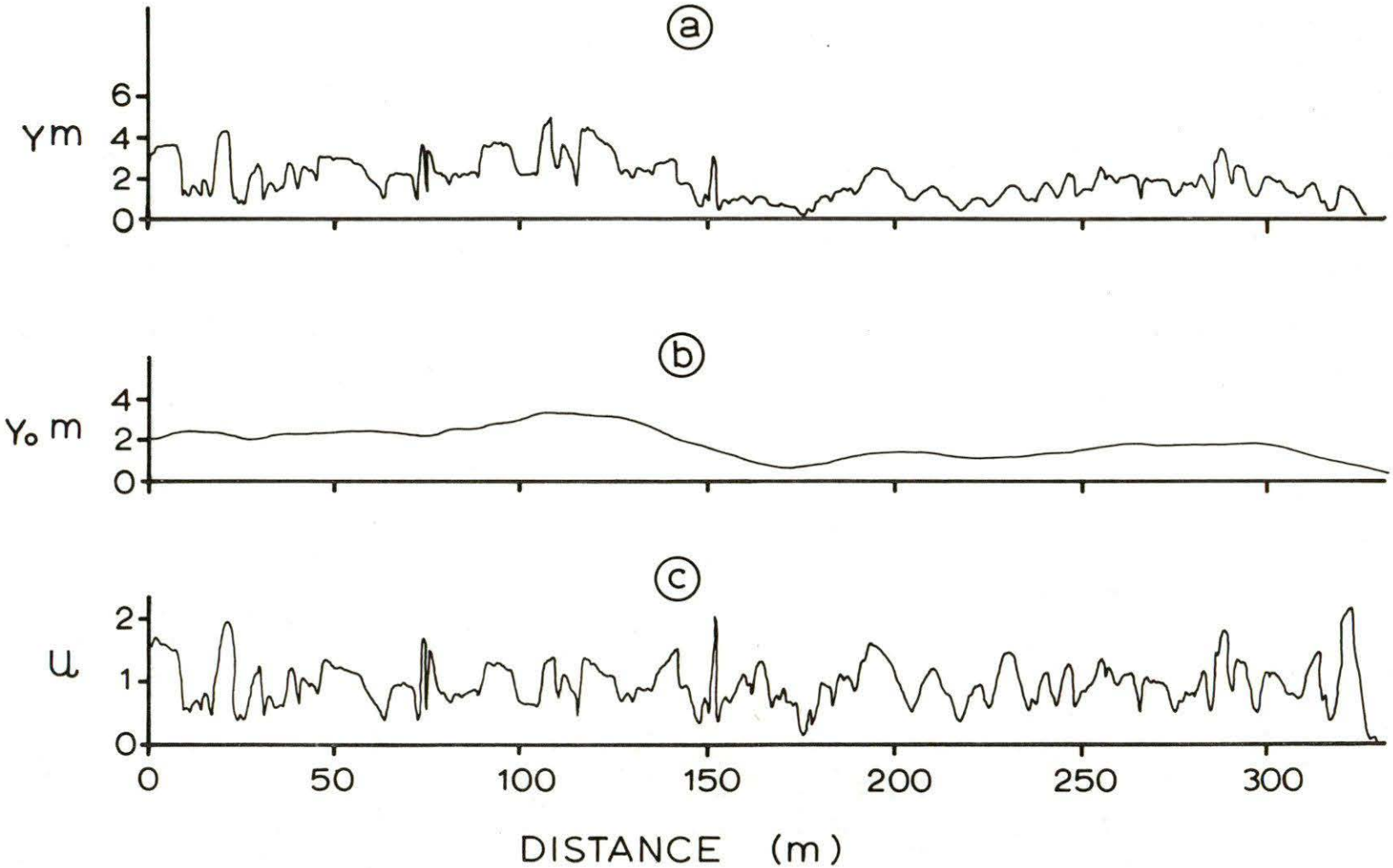

Fig. 18. UARS sonar profile. (a) Output of profiler 2, (b) Low-pass profile, (c) Normalized profile.

from a Gaussian function, with an excess of high peaks and a deficit of deep troughs. This is partly because no point is likely to have $y<0$, so that troughs deeper than a certain multiple of $\sigma(y_0)$ are impossible; this tends to generate a Rayleigh distribution. Also, in a keel composed of angular random blocks, a steep-sided trough tends to be shadowed by neighbouring blocks or even concealed by a block protruding under it, whereas steep peaks are free to stand clear. Predictions of trough depths attempted on the basis of Cartwright and Longuet-Higgens were found to give serious over-estimates.

Figure 20 shows that the local standard deviation $\sigma(y_0)$, for points $y(x)$ having y_0 in the ranges 0 - 0.5 m, 0.5 - 1.0 m, etc. shows an increasing trend when plotted against the mean depth of the points in each category. This suggests that we can "normalize" the profile by transforming the depths to

$$u(x) = y(x)/y_0(x) \qquad \ldots(17)$$

and we can then make predictions from the normalized depth profile which will be approximately valid for keels of any mean depth. This procedure is rigorous only if $\sigma(y_0) \propto y$ and (frequency of peaks) $\propto y_0$. Neither condition is fulfilled, but we still expect that the results will be of value over a restricted range of ridge types. Figure 18(c) shows $u(x)$ for profile 2.

The quantities $\hat{u}_{max}(\ )$, $\hat{u}_{min}(\ )$ were computed for all possible linkages ℓ, where

$$\hat{u}_{max}(\ell) = \frac{1}{N} \sum_{n_1=1}^{N} u_{max\ n_1,\ \ell} \qquad \ldots(18)$$

$$\hat{u}_{min}(\ell) = \frac{1}{N} \sum_{n_1=1}^{N} u_{min\ n_1,\ \ell} \qquad \ldots(19)$$

$$\ell = n_2 s \qquad n_2 = 1, 2 \ldots (N-1) \qquad \ldots(20)$$

In these equations

ℓ =	keel linkage over which maximum or minimum is estimated
N =	total number of data points (1024)
s =	interval between contiguous points (0.325 m)
$u_{min\ n_1,\ \ell}$ =	minimum value of u in a linkage ℓ beginning at the n_1-th point
$\hat{u}_{min}(\ )$ =	expectation of minimum value of u in a linkage ℓ (maximum values defined similarly).

A linkage such that $(N-n_1)<n_2$ was computed by repeating the record from the start; in this way every data point was given equal weight in the computation of equations (18) and (19).

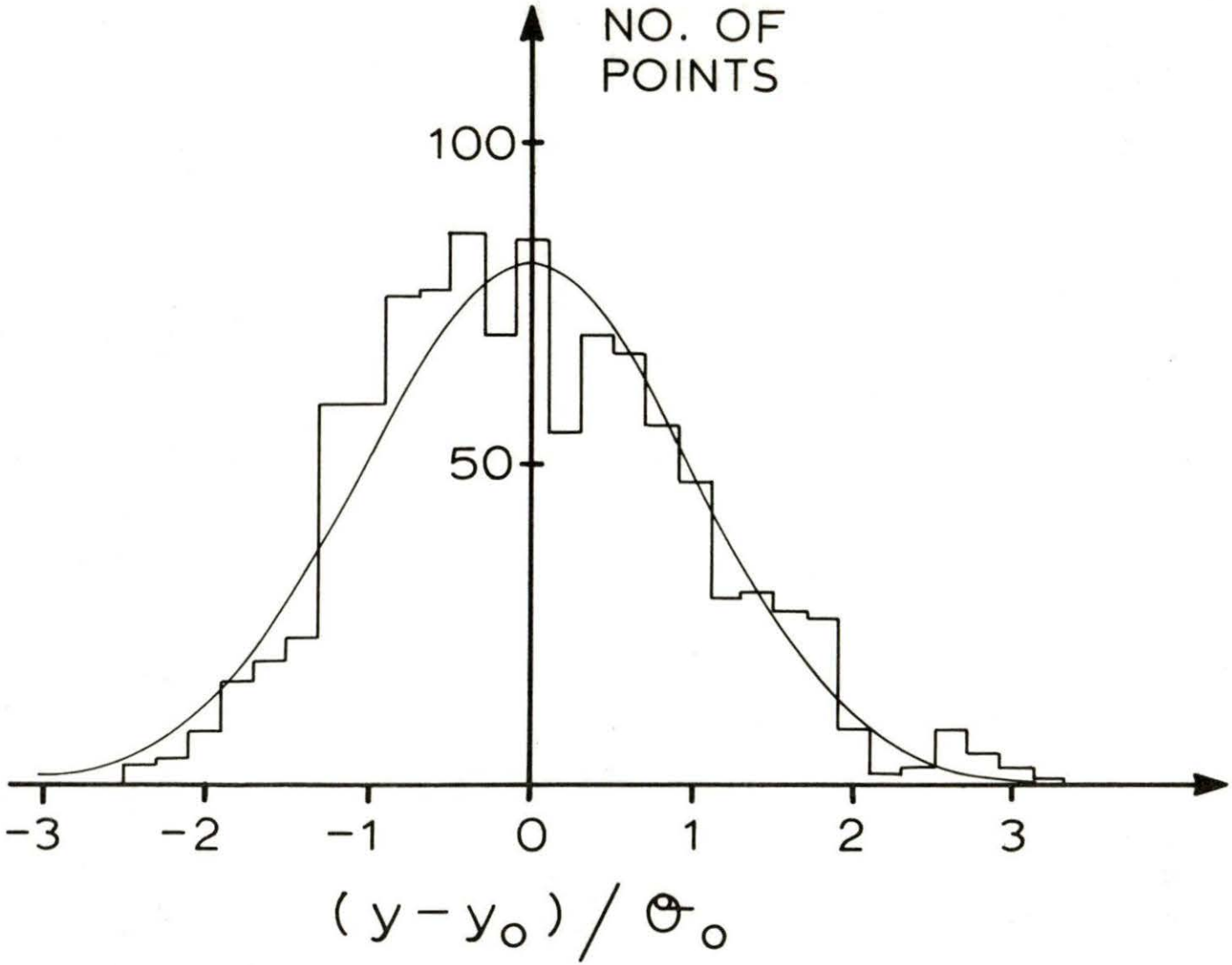

Fig. 19. Profiler 2, distribution of depths relative to local mean.

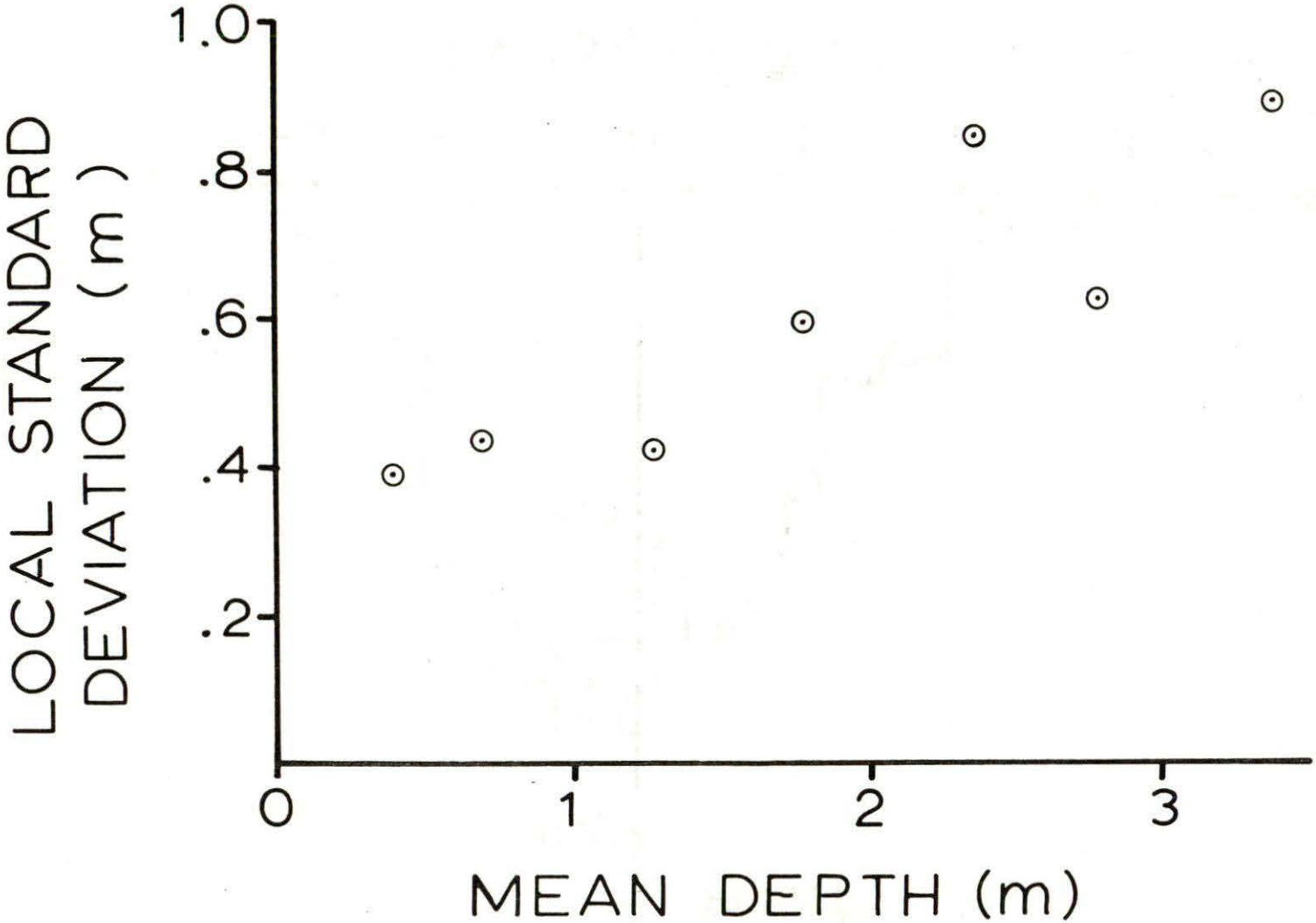

Fig. 20. UARS profiler 2, local standard deviation against local mean depth.

Figure 21 shows the results for both profiles. For small linkages there is symmetry between u_{max} and u_{min}, which is to be expected if the record really were a Gaussian random process. On this scale we are looking at the depth variations of a single ice block in the keel crest. At a linkage of about 13 m the u_{min} curve begins to flatten out more rapidly than the u_{max} curve; this is shown clearly in the magnified Figure 21(b) covering the first 26 m. Also at 13 m each curve (Figure 21(a)) shows a distinct knee, where the initial rapid deviation from unity turns into a gentler progression (the negative values of u_{min} for profile 1 at high ℓ are caused by a single trough whose draft is less than the mean of the level ice). It is clear, then, that 13 m represents a horizontal length scale for the size of ice blocks composing the keel, a scale which can be confirmed visually by inspection of Fig. 18(a). Thus, if a submerged observer travels 13 m along the keel crest he will surmount a single ice block and will encounter depths that vary between about 0.4 and 1.6 of the mean depth. If he is looking for a further comparable increase in the range of depths, to 0.0 and 2.4, he must travel at least 300 m, which is a typical survival distance for a ridge before it is crossed by another ridge.

It is likely that every ridge has its own length scale, which depends, among other things, on the nature of the ice that was used to build the ridge and the mode of ridge formation. Koerner (1970) found that 87% of ridges he examined in the Arctic Ocean were made of slabs with a thickness of less than 1 m, and 66% were less than 30 cm thick. The raw material for most ridges is therefore young ice existing in refrozen leads. Parmerter and Coon (1973) have shown how the dimensions of a ridge built by a given stress depend on the width of the lead and the thickness of the young ice within it, but their model cannot predict the size of ice blocks in the keel, and only sonar profiles can display this important quantity. A scale of 13 m is large, and suggests either that the ridge was built of thick ice slabs (i.e. by direct grinding of two multi-year floes) or that the profile has been smoothed by a long period of ablation.

The u_{min} curve in Fig. 21 should be treated with reserve. Figure 22 shows profiles 1 and 2 plotted together, and it can be seen that a trough in one profile is often covered by a peak in the other. This may imply the existence of a channel slanting through the keel, which would be permeable to oil, or there may be a lateral as well as a longitudinal structure of blocks, so that troughs shown in a single profile do not penetrate the whole width of the keel. The keel that we have examined has a relief of about 3 m and a block diameter of 13 m. It is also a shear ridge, whose formation typically does not involve the piling up of a great heap of blocks. Therefore it is reasonable to assume that the keel relief is one of individual blocks, lying at random angles, but strung out more or less in single file. A trough shown in one profile probably penetrates the whole keel, albeit at an angle so that a profile offset by 4.4 m does not show the trough in the same place. Thus the "universal" normalized curve of Fig. 21 can be used to predict minimum depths for shallow shear ridges not more than, say, 8 m in total draft, and it shows that such ridges are probably quite permeable to

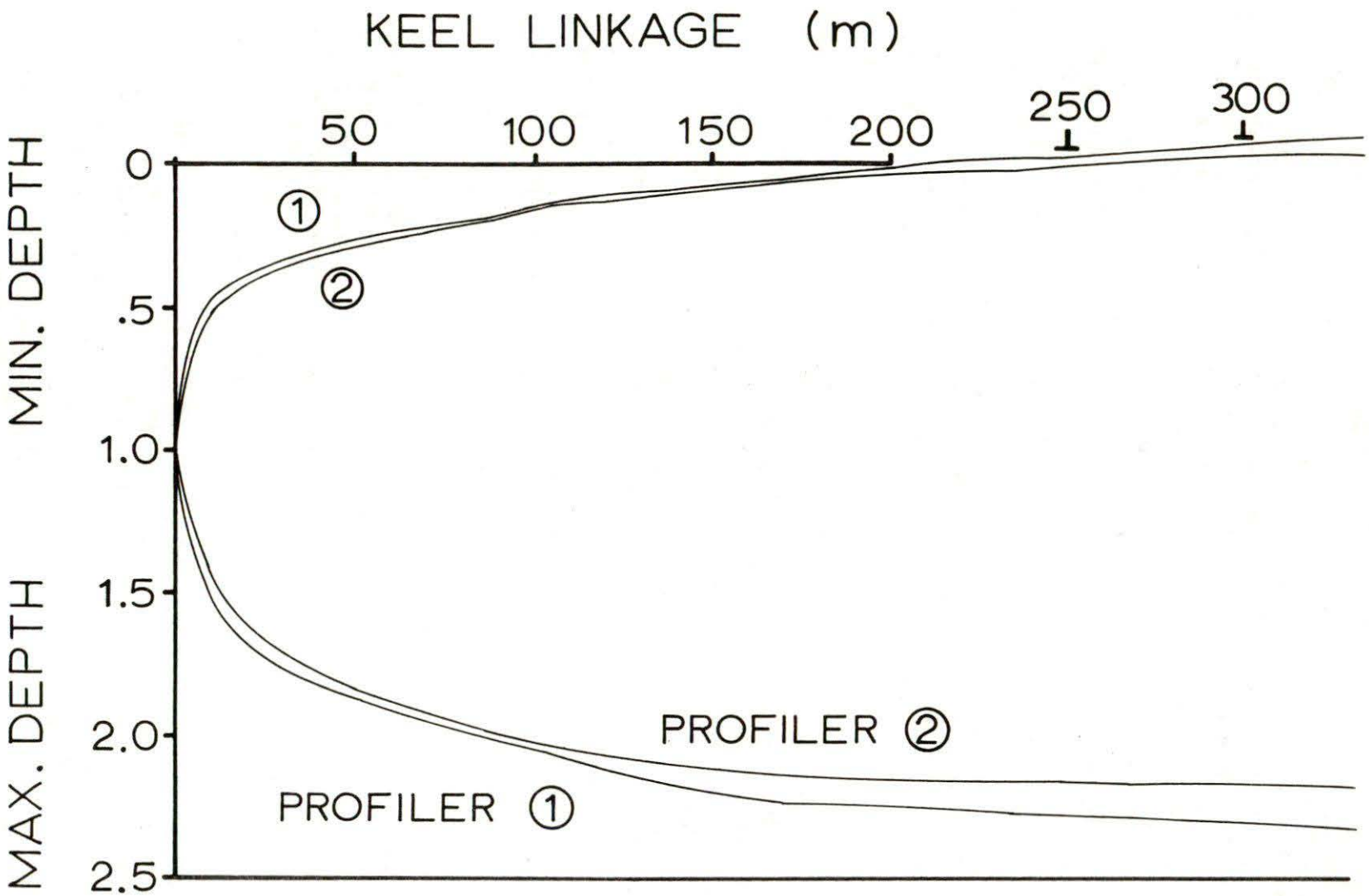

Fig. 21(a). Expectation of extreme depths against keel linkage.

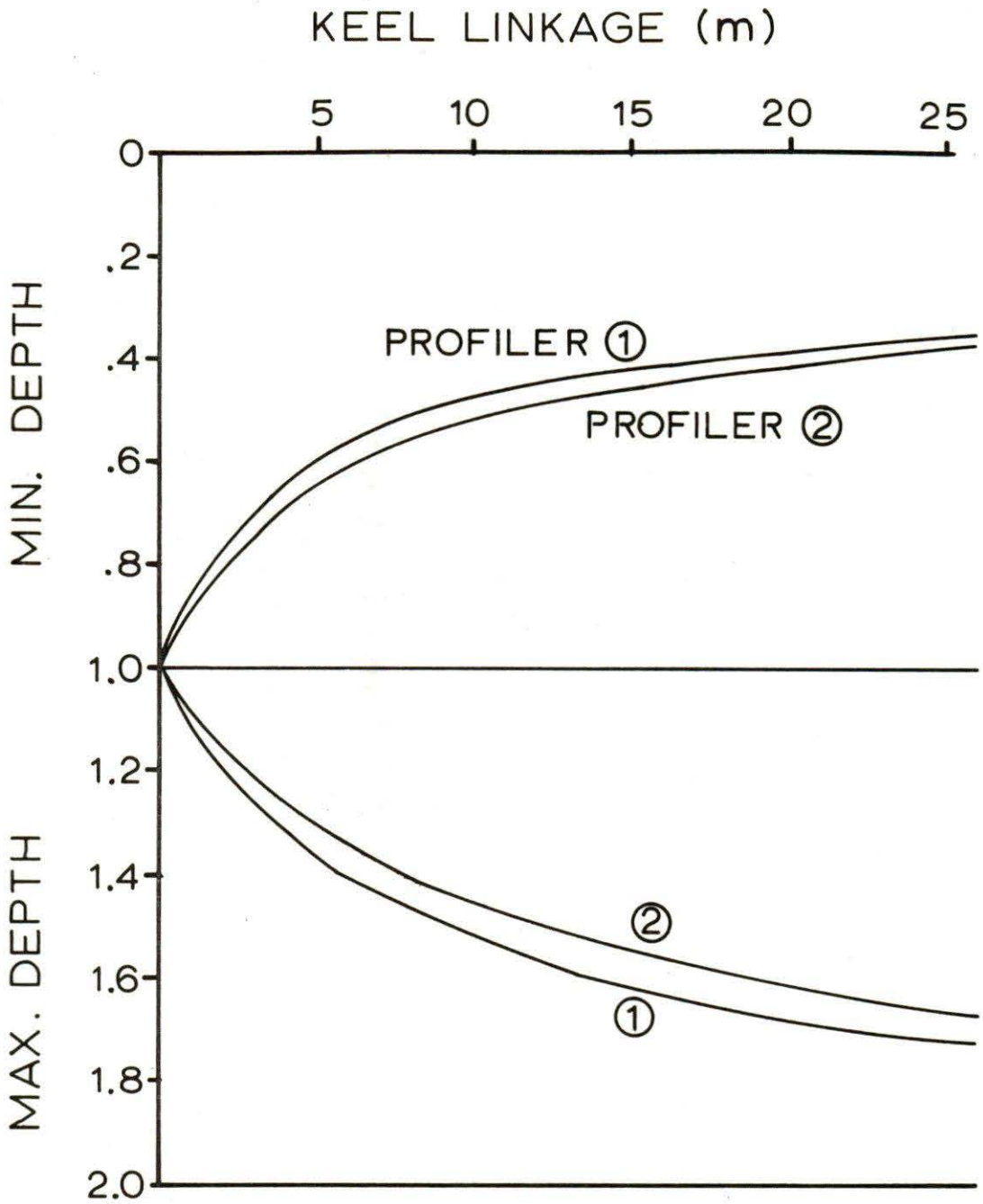

Fig. 21(b). Expectation of extreme depths at low keel linkages.

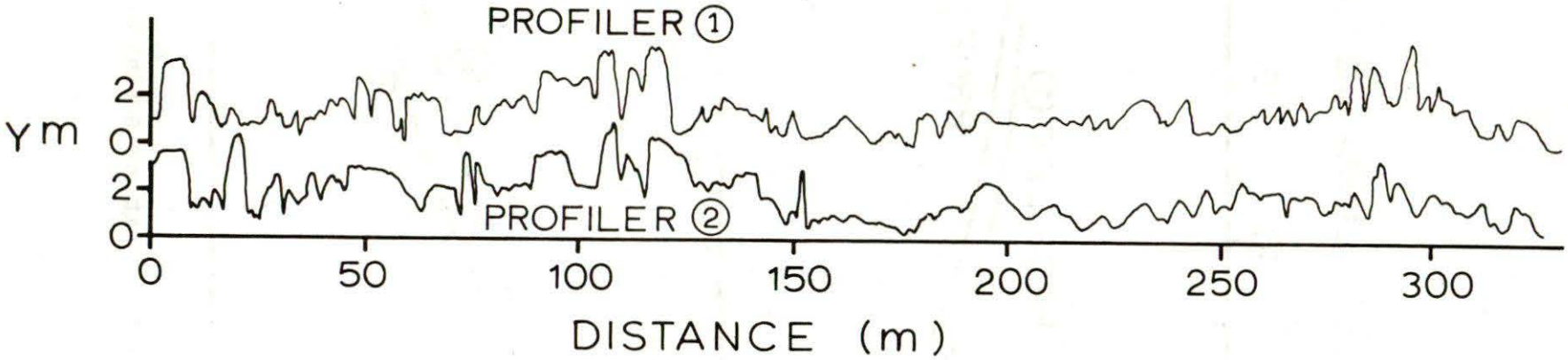

Fig. 22. UARS profiles 1 and 2.

oil. The results may also apply to shallow pressure ridges built of single blocks, but deep pressure ridges must have far lower relative depth fluctuations, although the absolute fluctuations are probably of similar, or greater, magnitude. As a rough guide, then, we can expect a very deep keel to show fluctuations of at least ±2 m about the mean draft, the deeper spurs being the first to gouge the sea bed when the keel moves into shallow water.

6. EFFECT OF MORPHOLOGY IN OIL CONTAINMENT

6.1 Volume and Nature of oil Release

The most severe type of accident that could occur would be the blowout of an exploratory well near the end of the summer drilling season, such that it could not be closed off until the following year. According to oil industry sources, the type of oil-bearing structure found in the Beaufort Sea could be expected to give an initial flow rate of some 2500 bbl/day^{-1} (400 m^3 day^{-1}), reducing after a month to a steady rate of 1000 bbl/day^{-1} (160 m^3 day^{-1}). Integrated over a year, this yields 4 x 10^5 bbl of oil (6.4 x 10^4 m^3), which we may take as a standard blowout scenario". Actual exploratory drilling may, of course, show flow rates that are quite different from this. It should be noted that the "Torrey Canyon" disaster released about 7 x 10^5 bbl of oil. An estimated 800 ft^3 (23 m^3) of free gas per barrel of oil is also expected from a blowout, and it is shown in Topham (1975) how this will generate a forced convection of water which will melt a large pool over the site of the blowout.

In addition to a severe, but unlikely, accident of this sort we can expect small accidental releases of oil from various sources on and around rigs. These will occur with increasing frequency as production begins. It has been written of a fully-developed offshore field (Alpine, 1971): -

> "Spills varying in size from a few gallons to many barrels are endemic to the Gulf of Mexico . . . U. S. Coastguard's reconnaissance flights report 3 to 7 pollution incidents every week."

In 1971 there were 1436 pipeline breaks in U.S. coastal waters, spilling 897,685 gallons of oil (Boesch et al, 1974), an average of 625 gallons (19 bbl) per spill. Most of these breaks arose from nearshore corrosion of old pipelines; corrosion in arctic waters is very slow, but there is the additional danger of pipeline disturbance by ice keels. Another source of minor spills will be the vastly increasing density of shipping in the Beaufort Sea, especially supply vessels and icebreaking tenders. These may lose oil from engine cooling loops, propeller shaft glands, leaks while fuelling from tank barges, etc.

Thus, in the absence of major accidents we can still expect a release of oil into the environment, perhaps of order 100 bbl/year. Our remarks on the spread of oil from a major blowout can also be taken to apply, on a much reduced scale, to the fate of oil from these minor releases.

. 54

6.2 Inner Fast Ice Zone

The simplest type of ice morphology is just a smooth, level ice sheet, as is found in the inner part of the fast ice zone. We assume that the various phenomena occurring directly over the blowout site (burning of oil in situ, damming by the melted-out pool, mixing and emulsification into the water column) have not prevented a significant fraction of the oil from spreading beyond the immediate limits of the blowout zone. The blowout site is visualized on this scale as a point source emitting a uniform flow of non-emulsified oil which is presented directly to the surrounding ice surface (i.e. emulsified and dispersed oil is assumed to come out of the water column relatively quickly and join the oil which is spreading across the ice surface). Assuming that the oil forms a coherent slick, and the evidence is that although the emitted stream may begin to spread as droplets, these tend to join up into lenses and then slicks (Keevil and Ramseier, 1975), our problem is to estimate the slick thickness and thus the oiled area per unit volume emission.

The author took part in the offshore oil spill experiment carried out by NORCOR some 30 km from Cape Parry on April 8, 1975 (Dickins et al, 1975). The first of the two spills was under a smooth ice floe, and the oil came to rest in a coherent slick of thickness (0.56±0.08) cm. The oil was Norman Wells crude, and studies by Rossenegger (1975) and Mackay et al (1975) have shown that this is the equilibrium thickness of a drop or lens of Norman Wells crude lying at rest under an ice sheet. The thickness of a lens of large diameter is given by the balance of surface tension versus buoyancy forces around the edge of the lens: -

$$H^2 \delta\rho g = 2\,T(1 - \cos\theta) \qquad \ldots(21)$$

where $\delta\rho$ = density difference between oil and sea water
T = surface tension at oil/ice interface
θ = oil/ice contact angle, measured within the oil

Norman Wells crude has a specific gravity of 0.847, but its other properties appeared to be quite variable, presumably due to the presence of surfactants. It was found that the surface tension, especially, had a wide range, but that the most common values were between 1.5 and 10^{-2}N m^{-1}, with θ in the range 140° to 170°. This gives a range 0.55 to 0.68 cm for H. Beaufort Sea oil may have different properties than Norman Wells, and other oils tested seemed to have a higher H, up to 1 cm. We therefore take 0.5 cm to 1.0 cm as a feasible range for H, with 0.56 cm as our favoured value. It should be noted that Wolfe and Hoult (1974) offered a value of 0.7 cm, but this was based on heat flow reasoning which ignored surface tension. The area covered by various volumes of oil can now be estimated: -

TABLE 8

Volume	Area		
	H = 5 mm	5.6 mm	10 mm
1 barrel (0.1591 m^3)	31.9 m^2	28.4 m^2	15.9 m^2
1 cubic meter	200 m^2	179 m^2	100 m^2
4 x 10^5 bbl ("1 blowout")	12.7 km^2	11.4 km^2	6.4 km^2

The actual dimensions of the slick depend entirely on the surface currents during the period of the oil release. The Cape Parry spill took place in a current of 0.10 m s^{-1}, and although this current defined the direction of spread it did not cause the oil to continue spreading after it had reached its equilibrium thickness. The final shape of the slick could be idealized as an elongated ellipse with the spill point as one focus and the major axis pointing downstream. On this reasoning, in an area of steady currents a "standard blowout" would cause a slick roughly 6 km by 2 km, the longer axis pointing downstream. However, currents are never steady, certainly not for a period of a year, so the actual shape of the slick is indeterminate. Once the slick has reached its equilibrium thickness the spreading stops and, in winter, the oil becomes fixed by new ice growing below it and through it. If the source sends out oil in pulsations one can envisage a fresh ice surface which has sandwiched one slick acting as the collecting surface for a second slick, thus building up a multi-year sandwich and reducing the oiled area per unit volume. The extent to which this can happen is uncertain, because as each layer is added the very low thermal conductivity of the oil will cause the rate of ice growth to decrease considerably. We assume that gas will vent through the hole generated directly over the blowout.

For the inner shorefast ice zone, then, we have a reasonable idea of the area that will be affected by a blowout provided it occurs after freeze-up. The dimensions of the affected area are quite small, and provided the oil does not spread as far as the tidal cracks it will sit in place throughout the winter. Unfortunately such oil is not easily acessible for clean-up, since ice growing through the oil tends to divide the slick into cells, making drilling and pumping ineffective. Of critical importance is the date of break-up of the shorefast ice: NORCOR and other studies have shown that in early summer the oil migrates to the upper ice surface through expanded brine drainage channels, making it available for clean-up, but if this happens after break-up the oiled floes will become widely distributed and the oil may find its way onto the open sea.

6.3 Outer Fast Ice Zone

The outer fast ice zone is characterized by a morphology of ridges and hummocks, but the ice itself is stationary. In this case the morphology acts to reduce the area of the spill and to make clean-up easier. Kovacs and Mellor (1974) describe fields of severe rubble or hummocking in this zone, generated in early fall by pressure of the polar pack on the young fast ice. Such a zone is the least unpleasant place for a blowout to occur, provided most of the oil release occurs after the rubble field has consolidated itself (otherwise the oil will become intimately bound up in the deformed ice). In such a field one can easily imagine a roughness scale of 5 cm on the ice bottom; the oil will collect in pools and pockets whose position can be estimated from the top surface morphology and which can more easily be tapped and pumped out. The actual area affected will be less, only 1.3 km^2 for a standard blowout in an area of vertical roughness scale 5 cm. Elsewhere in the outer fast ice zone the ridging will also act to reduce the area of a spill, but to a lesser extent.

The rough ice in this zone can be seen in Fig. 23, which is SLAR imagery taken in Mackenzie Bay during the Argus flight of April 26, 1975. The smooth inner fast ice zone, spreading from the shore, is criss-crossed by ice roads serving artificial islands, there is then an outer zone of rougher ice before the wide lead noted in Section 3.3 marks the transition to moving ice.

6.4 Shear Zone

In the shear zone the real problems begin. First, the 20 m contour itself would be an extremely hazardous place to have a blowout, because a wide lead opens here early in the spring, allowing the oil to spread freely into open water and to distribute itself over great distances. Further out into the winter shear zone we find heavy ridging, many leads, and vigorous and rapid ice movement. The measurements of Hibler et al (1973, 1974a) have shown that under wind stress and internal stress transmitted from the polar pack there can be rapid shearing motions as well as alternate convergence and divergence of the pack in periods as short as a day, which cause opening and closing of lead systems. The long-term average motion of the ice is westward with the Beaufort Gyre, and from the drift track of ice island T-3 in this area (Campbell and Martin, 1973) we estimate a long-term drift of about 1000 km/year with a complete circuit of the Beaufort Gyre in 7 to 10 years.

In such an area, the first question concerns the scale of a blowout in relation to the frequency of leads and ridges. Figure 24 is a SLAR image which shows the very sharp tracery of intersecting ridges found in first-year ice; Figure 25, from further north, shows a much more complex mixture of first and multi-year ice with leads, rafting and rubble fields. We can approximate the ice conditions by assuming that, except for pressure ridges and leads, the ice surface is smooth with the oil containment factor given in Table 8. Let us consider first a simply connected environment, the smallest space scale that consists only of smooth ice. If μ is the mean number or ridges per km, such a scale has a mean diameter of $1/\mu$ and, supposing it is square, is surrounded by a length $4/\mu$ of ridging. We need to estimate a specific containment factor $\bar{V}$ for a ridge, defined as the mean volume of oil that can be retained per unit ridge length. This is an extremely difficult quantity to estimate. The laboratory experiments of Moir and Lau (1975) suggest that oil will not build up behind a ridge as it does behind a boom in open water, but that instabilities will arise which allow the oil to pass under the keel. A full-scale experiment is needed to see whether this happens in practice. The nearest approach to such an experiment was the second offshore spill at Cape Parry, made near a small pressure ridge. Unfortunately the quantity of oil spilled was inadequate to test whether the pool that was growing behind the ridge would continue to grow without instability. The pool was formed because of the presence of a depression in front of the keel, a long wave-like feature that either represented part of the keel structure or else was generated by differential ice growth due to snow drifting against the surface ridge. If a keel is indeed ineffective as a boom it may still have a large containment factor due to the presence of such deformed ice in its "foothills".

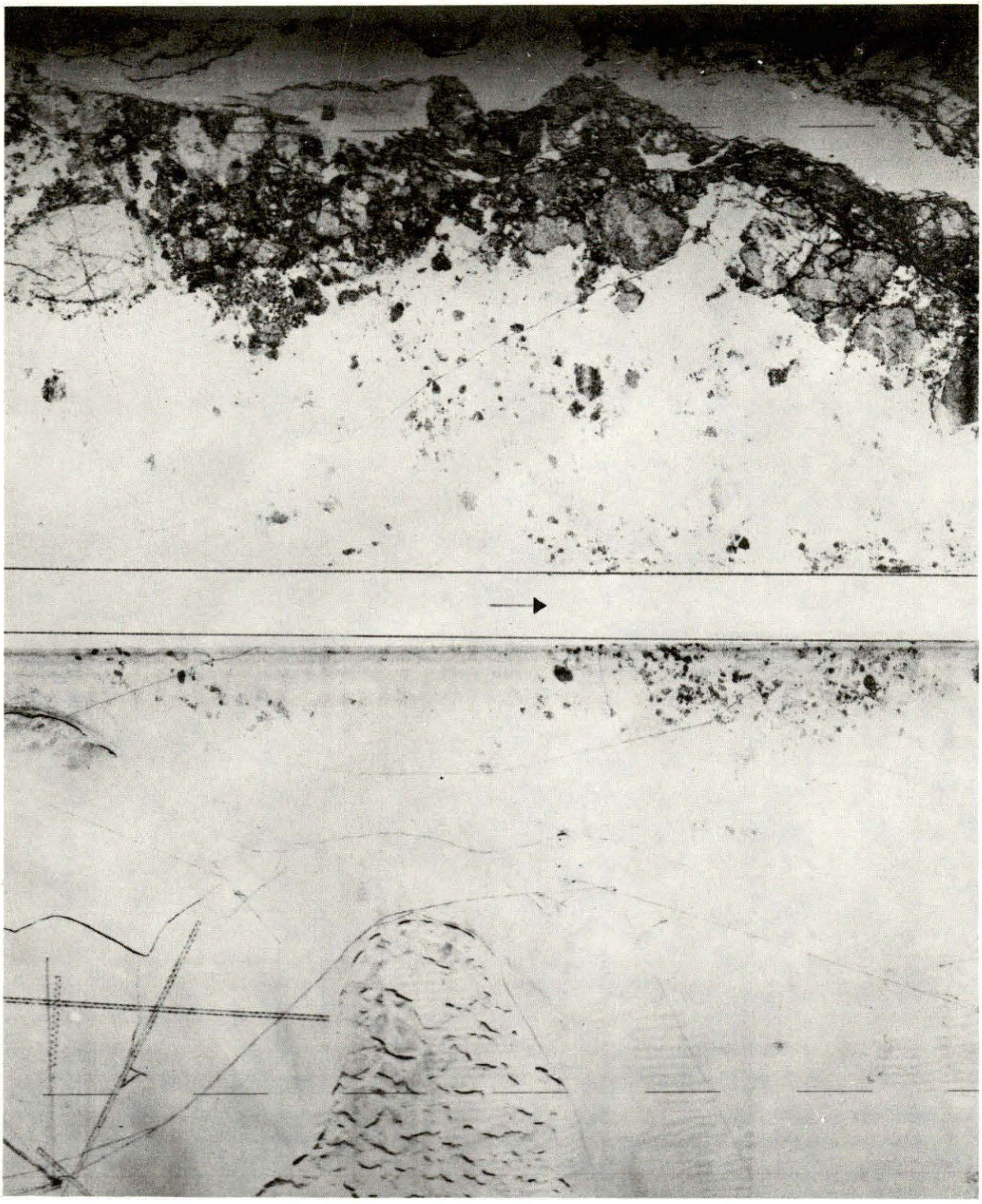

Fig. 23 SLAR imagery, 26 April 1975. Scale 1:250,000. Aircraft heading 052°, centre of picture 69° 49' N, 134° 23' W. Smooth fast ice near shore, with vehicle tracks; scattered floes embedded in fast ice further from shore; rough ice in outer fast ice zone; then wide lead marking edge of shear zone. North end of Richards Island at bottom; Hooper Island at extreme left.

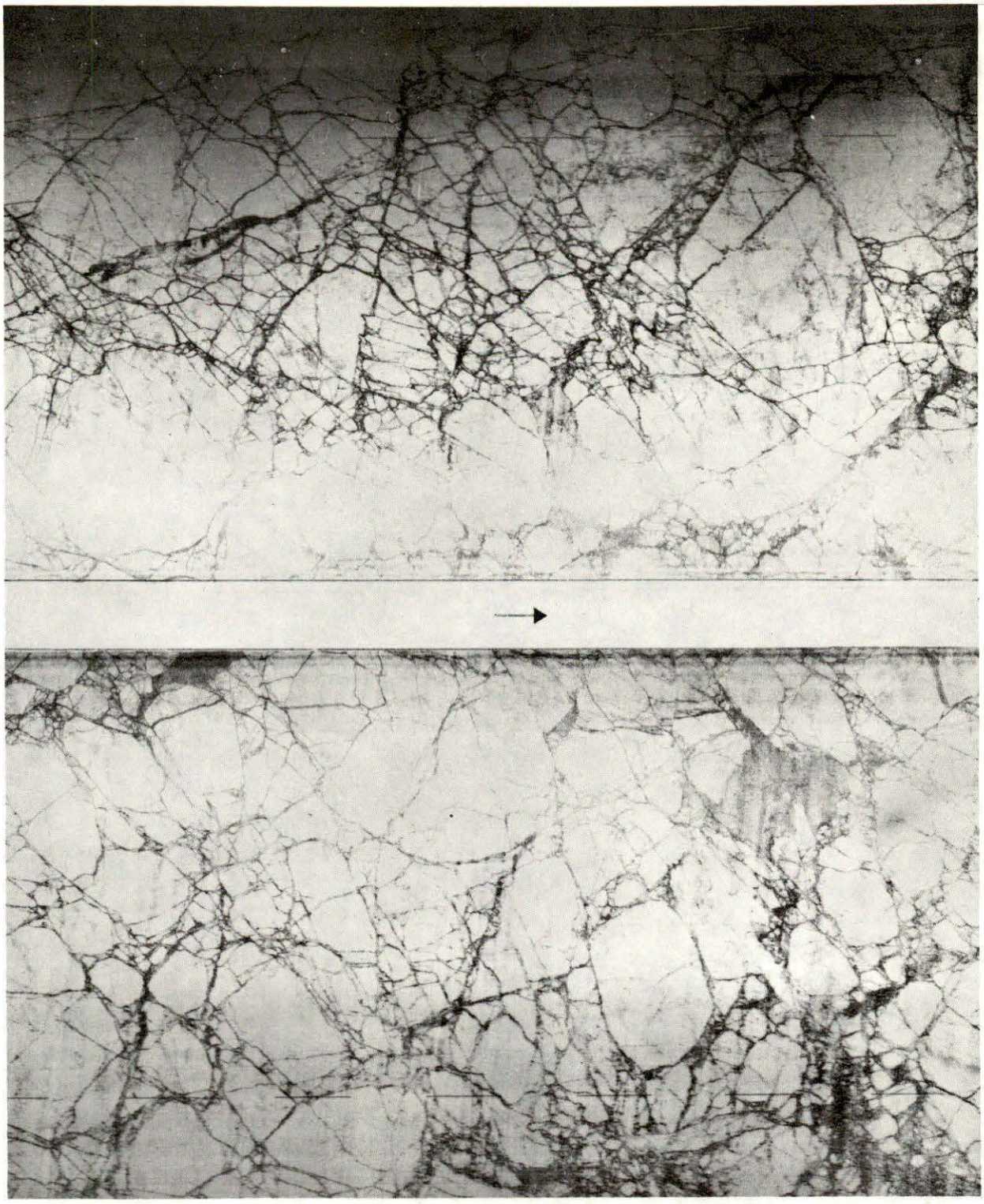

Fig. 24 SLAR imagery, 26 April 1975. Scale 1:250,000. Aircraft heading 052°, centre of picture 70° 56' N, 134° 30' W. First-year ice in shear zone with linear tracery of pressure ridges.

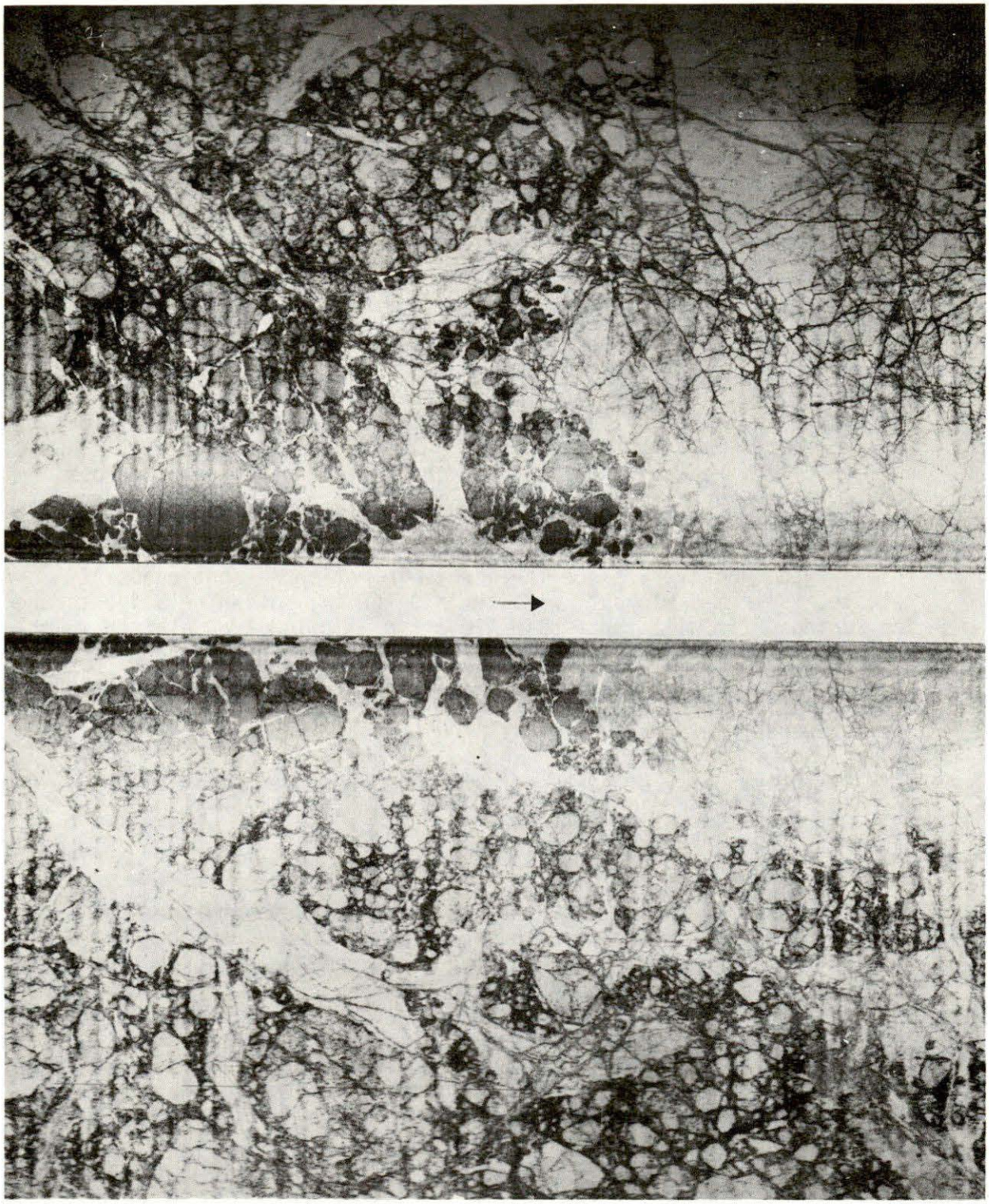

Fig. 25 SLAR imagery, 26 April 1975. Scale 1:250,000. Aircraft heading 180°, centre of picture 71° 54' N, 139° 00' W. Polar pack, with smooth floes (light) and rough, possibly multi-year, floes (dark), rubble fields (black matrix around floes) and polynyi (white).

Unfortunately insufficient keels have been profiled to determine whether these depressions are a universal phenomenon. As a basis for speculation we may consider the actual pool developed in the Cape Parry spill as being typical. According to the diver, its dimensions were 6 feet in width by 4 inches deep, giving $\bar{V} = 0.9\ m^2$ per meter linkage. Our simple environment thus has an area of $1/\mu^2$, which can contain a volume H/μ^2 of oil under its level ice. Its bounding ridge can retain $4\ \bar{V}/\mu$ of oil. Taking 9 ridges per km as typical of heavy ridging, and H as 0.56 cm, we have an area of 12,000 m^2, which has a capacity of 69 m^3 of oil (434 bbl) under level ice, and 84 m^3 (528 bbl) retained against ridges. Thus more oil is contained against ridges than under the level ice, especially as we would normally expect $\bar{V}$ to be much greater than our estimate.

We have still to consider leads and the effect of ice motion. Taking the figure found in our aerial survey (0.72 leads per km) as typical, we have approximately one lead per 5 - 10 ridges. Thus if oil is spilled at a fixed point relative to the ice, it will have to cross about 3 to 5 ridges to reach a lead, i.e. 3 to 5 simple environments which will require between 2900 and 4800 bbl of oil. A small instantaneous spill, even in the shear zone, is therefore unlikely to get into a lead. However, since the ice is in motion, a continuous release, as from a blowout, will be in perpetual motion relative to the ice surface. It will thus "paint" a strip of oiled ice, a strip which will become more sinuous and Gordian in character the further it progresses from the "paintbrush". The oil will enter leads, and as lead systems are created and destroyed it will become incorporated into the subsequent new pressure ridges.

If V is the velocity of ice drift and Ω is the rate of oil emission, the width W of the oiled swath traced out in smooth ice is given by

$$W = \Omega/VH \qquad \ldots(22)$$

W varies inversely with V, so that the swath progressing from the blowout site grows wider when the ice drift slows. The long-term mean drift in the eastern and southern Beaufort Sea has been given as 2.2 and 2.6 km/day by Coachman and Barnes (1961); 2.7 km/day from the drift track of T-3 taken over a year (Campbell and Martin, 1973); and 2.4 km/day from a year's average of monthly means (Coachman, 1969). The monthly means in the last reference shows an increase to about 4 km/day in September and October, the months of lowest ice concentration when rapid response to wind stress is possible. All of these long-term means are much lower than the instantaneous mean velocity which is required for Equation (22). Dunbar and Wittman (1962) defined the difference in a <u>coefficient of meandering</u>, the ratio of net distance covered to a long-term distance made good, which they calculated for various ice stations. The only one in the southern Beaufort Sea was T-3 (1959-69 drift), with a coefficient of 2.0, but other coefficients in the Beaufort Gyre ranged from 1.5 to 10.0 with a mean of 3.9. The shear zone to the northeast of Mackenzie Bay, where drilling is proposed, exhibits rapid ice movement in spring and summer, with frequent eastward excursions of the pack; using satellite photographs Marko(1975) reports velocities of 10 km/day or

more as common. We conclude that the long-term westward drift of about 2.4 km/day should be multiplied by a meander coefficient of between 2 and 4 to obtain the actual distance travelled by the ice and hence V for equation 22. Taking the limits of Ω as 2500 and 1000 bbl/day, and the limits of H as 0.56 cm (smooth ice) and 2 cm (to include a containment factor for ridging) we obtain the following estimates for W: -

TABLE 9

Ω bbl/day	V km/day	H cm	Swath width W m
1000	4.8	0.56	5.9
1000	4.8	2.0	1.7
1000	9.6	0.56	3.0
1000	9.6	2.0	0.8
2500	4.8	0.56	14.8
2500	4.8	2.0	4.1
2500	9.6	0.56	7.4
2500	9.6	2.0	2.1

It is clear that W is small under all possible assumptions, and in fact in moving ice it is no longer valid to consider the blowout site as a point source. Topham (1975) found that bubble plumes in 23 m and 60 m of water generated circular areas of diameter 40 m and 72 m respectively at the water surface, which were swept by the bubble field and which constitute the "point source". A blowout in which oil and gas come up together would emit oil to the environment from the edges of this highly turbulent area. The two depths are typical of the inner shear zone and are quite close to the depths of the proposed 1976 drilling sites. Since the diameter of the source exceeds the width of a fully-oiled swath we draw the important conclusion that the paint-brush does not have enough paint to draw a full black line, i.e. the swath will take the diameter of the source rather than W and will not be oiled to its full carrying capacity. There will be a patchy oil coverage over this wider swath, but the patchiness will be distributed over a greater area. Consider a blowout in 60 m of water. The swath is now of minimum diameter 72 m, and with a 9.6 km/day drift the area of ice affected in a year is 252 km^2, twenty times the area estimated in Table 8 for a stationary ice cover. Within this area the oil contamination is equivalent to a continuous cover of thickness only 0.06 cm (at 2500 bbl/day). Not only is the swath wider and more patchy, but the meander results in a very sinuous swath track which may spread 1000 km to the westward in a year yet be 2000 to 4000 km long. In this way a low concentration of oil is distributed over a very wide geographical area, both in latitude and longitude, making clean-up extremely difficult.

On this new view a keel has no special status; since the oil coverage is insufficient to build a coherent slick of equilibrium thickness under smooth ice, there is no incentive for the oil to pile up behind keels.

. 62

Depressions near keels will still act as gathering points for oil deposited in their "watershed area", but the efficiency of collection is less than if the oil were positively spreading. Thus drilling and pumping in the neighbourhood of ridges is not likely to be very effective. In addition we must consider the effect of gas, which in stationary ice vents from a hole directly over the blowout. With moving ice it is not known whether the gas will spread under the ice until if finds a crack, or whether its pressure will continually break the ice over the blowout, resulting in a trail of shattered ice blocks and brash ice which coincides with the oiled swath. Icebreaking experience with the Alexbow has shown that it is far easier to break ice from below than from above, and pressures of 0.1 atm. have been quoted as sufficient. If continual breakage occurs much of the oil will end up mixed in with the loose blocks and brash ice; it will be accessible for clean-up for a few hours before becoming frozen into a matrix of fresh ice (Lewis, 1970). If breakage does not occur, the spreading gas may fill pockets and depressions in the ice bottom, destroying the containment factor of a keel completely.

With an essentially random mechanism for oil deposition the percentage that will enter existing leads will be only slightly greater than the percentage coverage of open water, since drainage into leads from the periphery of floes is only a local phenomenon. Thus in winter less than 5% of the oil will be deposited in existing leads. In summer, as seen in Fig. 3, almost all the oil will be in open water if the blowout site is south of the summer ice margin, while if the site is well inside the ice margin it may only be 10%. In winter the existing leads will close within a few days, and the young ice and oil in them will be built into pressure ridges. We thus expect to see oiled pressure ridges, with a weaker structure than normal ridges which will be an early source of oiled meltwater pools in summer. Leads which open in an oiled ice cover after deposition has occurred will accumulate little oil, since once the oil has frozen in, its capacity for horizontal movement or drainage is slight. The "lead-matrix pumping" mechanism of Campbell and Martin (1973), whereby closure of one set of leads pumps oil longitudinally into another set of leads, is not likely to occur since lead closure takes place initially at a chain of contact points which retain the oil so that it is either built into the ridge or forced over or under the adjacent level ice.

REFERENCES

Ackley, S., W.D. Hibler III, F. Kugzruk, A. Kovacs and W.F. Weeks (1974) Thickness and roughness variations of Arctic multi-year sea ice. AIDJEX Bull., 25, pp 75-96.

Alpine Geophysical Associates Inc. (1971) Oil pollution incident Platform Charlie, Main Pass Block 41 Field, Louisiana. Project 15080 FTO, Contract 14-12-860, Final rep.

Archibald, D.C. (1972) An aerial ice reconnaissance platform with remote sensors suitable for the Canadian Ice Reconnaissance Program. In Sea Ice, Proc. Intl. Sea Ice Conf., Reykjavik, Natl. Res. Council of Iceland, Reykjavid, pp 229-236.

Brochu, C.J. and R.T. Lowry (1975) Logiciel graphique interactif écrit en APL pour le traitement des données. Defence Res. Establ., Ottawa. Tech. Note 75-14.

Campbell, W.J. and S. Martin (1973) Oil and ice in the Arctic Ocean: possible large-scale interactions. Science, 181, pp 56-58.

Cartwright, D.E. and M.S. Longuet-Higgins (1956) The statistical distribution of the maxima of a random function. Proc. Roy. Soc. A. 237, pp 212-232.

Coachman, L.K. (1969) Physical oceanography in the Arctic Ocean: 1968. Arctic, 22(3), pp 214-224

Coachman, L.K. and C.A. Barnes (1961) The contribution of the Bering Sea water to the Arctic Ocean. Arctic, 14, pp 146-161.

Cooper, P.F. (1974) Landfast ice in the southeastern part of the Beaufort Sea. In The Coast and Shelf of the Beaufort Sea, Arctic Inst. of N. Amer., Arlington, Va., pp 235-241.

Dickins, D., J. Overall and R. Brown (1975) The interaction of crude oil with Arctic sea ice. Tech. Report, DSS Contract OSV4-0043, NORCOR Research and Engineering Ltd., Yellowknife, NWT.

Dunbar, Moira and W.I. Wittmann (1963) Some features of ice movement in the Arctic Basin. Proc. Arctic Basin Symposium, Hershey, Pa., Oct. 1962. Arctic Inst. of N. Amer., Washington, D.C., pp 90-104.

Francois, R.E. and W.K. Nodland (1972) Unmanned Arctic Research Submersible (UARS) system development and test report. Univ. of Washington, Applied Phys. Lab., Tech. Report APL-UW 7219, pp 88.

Francois, R.E. and W.K. Nodland (1973) Arctic acoustic measurements at 50 KHz. Univ. of Washington, Appl. Phys. Lab., Tech. Report APL-UW 7313, pp 35.

Gonin, G.B. (1960) Detection of the degree of ice hummocking by statistical analysis of aerial photography data. Problems of the Arctic and Antarctic, 3, Tr. Israel Prog. for Sci. Trans., Jerusalem.

Herbert, W.W. (1970) The first surface crossing of the Arctic Ocean. Geogrl. J., 136(4), pp 511-533.

Hibler, W.D. III, W.F. Weeks and S.J. Mock (1972) Statistical aspects of sea ice ridge distributions. J. Geophys. Res., 77(30), pp 5954-5970.

Hibler, W.D. III, W.F. Weeks, S.F. Ackley, A. Kovacs and W.J. Campbell (1973) Mesoscale strain measurements on the Beaufort Sea pack ice (AIDJEX 1971). J. Glaciol. 12, pp 187-206.

Hibler, W.D. III, S.F. Ackley, W.K. Crowder, H.L. McKim, D.M. Anderson (1974a) Analysis of shear zone ice deformation in the Beaufort Sea using satellite imagery. In The Coast and Shelf of the Beaufort Sea, Arctic Inst. of N. Amer., Arlington, Va., pp 285-296.

Hibler, W.D. III, S.J. Mock and W.B. Tucker III (1974b) Classification and variation of sea ice ridging in the western Arctic Basin. J. Geophys. Res. 79(18), pp 2735-2743.

Keevil, B.E. and R.O. Ramseier (1975) Behaviour of oil spilled under floating ice. Proc. Conf. on Prevention and Control of Oil Pollution, March 25-27, 1975, San Francisco, pp 497-501.

Ketchum, R.D. Jr. (1971) Airborne laser profiling of the Arctic pack ice. Remote Sensing of Environment, 2, pp 41-52.

Klimovitch, V.M. (1972) Characteristics of hummocks in shore ice. Met. & Hydrology, 5. Tr. by Department of Commerce, Washington, D.C. Joint Publ. Res. Serv. JPRS56595.

Koerner, R.M. (1970) Weather and ice observations of the British Trans-Arctic Expedition 1968-69. Weather, 25(5), pp 218-228.

Kovacs, A. (1972) On pressured sea ice. In Sea Ice, Proc. Intl. Sea Ice Conf., Reykjavik Natl. Res. Council of Iceland, Reykjavid, pp 276-295.

Kovacs, A., S. Ackley, W.F. Weeks and W.D. Hibler III (1973) Structure of a multi-year pressure ridge. In Investigations performed on the Arctic Ice Dynamics Joint Experiment, March 1971, U.S. Army Cold Regions Res. Eng. Lab., Hanover, N.H., Res. Report 315, pp 23-33.

Kovacs, A. and M. Mellor (1974) Sea ice morphology and ice as a geologic agent in the southern Beaufort Sea. In The Coast and Shelf of the Beaufort Sea, Arctic Inst. of N. Amer., Arlington, Va., pp 113-161.

Lewis, C.F.M. (1975) Bottom scour by sea ice in the southern Beaufort Sea. Beaufort Sea Project Tech. Report 23. Geological Survey of Canada, Department of Energy, Mines and Resources, Ottawa, Ont.

Lewis, E.L. (1970) In Report of the Task Force: Operation oil. Ministry of Transport, Ottawa, 2, pp 19.

Lowry, R.T. (1974) An experiment in ice profiling in Nares Strait and the Arctic Ocean. Symp. on Remote Sensing in Glaciol., Cambridge, Sept. 1974, Abst. publ. in J. Glaciol., 15(73), pp 462-463 (1975).

Lowry, R.T. and C.J. Brochu (1975) A system for the treatment of airborne laser profilometer data of ice. Defence Res. Establ., Ottawa, Tech. Note 75-15.

Lyon, W. (1967) Under surface profiles of sea ice observed by submarine. In Physics of Snow and Ice, Intl. Conf. on Low Temp. Science, Institute of Low Temperature Science, Hokkaido Univ., Sapporo, Japan, 1(1), pp 707-711

Mackay, A., M. Medir and D.E. Thornton (1975) Interfacial behaviour of oil under ice. In Press. Can. J. Chem. Eng.

Marko, J.R. (1975) Satellite observations of the Beaufort Sea ice cover. Beaufort Sea Project Tech. Report 34. In Press. Department of the Environment, Victoria.

Maykut, G.A. and N. Untersteiner (1969) Numerical prediction of the thermodynamic response of Arctic sea ice to environmental changes. RAND Corp., Santa Monica, Calif., Report RM 6093-PR, 173 pp.

Mock, S.J., A.D. Hartwell and W.D. Hibler III (1972) Spatial aspects of pressure ridge statistics. J. Geophys. Res. 77(30), pp 5945-5953.

Moir, J.R. and Y.L. Lau (1975) Some observations of oil slick containment by simulated ice ridge keels. Unpubl. Report, Canada Centre for Inland Waters, Burlington, Ont.

Parmerter, R.R. and M.D. Coon (1973) Mechanical models of ridging in the Arctic sea ice cover. AIDJEX Bull., 19, pp 59-112.

Pelletier, B.R. and J.M. Shearer (1972) Sea bottom scouring in the Beaufort Sea of the Arctic Ocean. In Marine Geology and Geophysics, Proc. 24th Intl. Geological Congress, Sec. 8, pp 251-261.

Reimnitz, E. and P.W. Barnes (1974) Sea ice as a geologic agent on the Beaufort Sea shelf of Alaska. In The Coast and Shelf of the Beaufort Sea, Arctic Inst. of N. Amer., Arlington, Va., pp 301-353.

Rosenegger, L.W. (1975) Oil-in-ice studies. Lab. report L-12075, Imperial Oil Co. Ltd., Resource Production and Technical Services Laboratory, Calgary, Alta.

Shearer, J. and S. Blasco (1975) Further observations of the scouring phenomena in the Beaufort Sea. Geological Survey of Canada, Dept. of Energy, Mines and Resources, Ottawa, Paper 75-1, Part A, pp 483-493.

Stringer, W.J. (1974) Morphology of the Beaufort Sea shorefast ice. In The Coast and Shelf of the Beaufort Sea, Arctic Inst. of N. Amer., Arlington, Va., pp 165-172.

Swithinbank, C.W.M. (1972) Arctic pack ice from below. In Sea Ice, Proc. Intl. Sea Ice Conf., Reykjavik, Natl. Res. Council of Iceland, Reykjavik, pp 246-254.

Topham, D.R. (1975) Hydrodynamics of an oil well blowout. Beaufort Sea Project Tech. Report 33, In Press, Dept. of the Environment, Victoria.

Tucker, W.B. III, and V.H. Westhall (1973) Arctic sea ice ridge frequency distributions derived from laser profiles. AIDJEX Bull, 21, pp 171-180.

Weeks, W.F., A. Kovacs and W.D. Hibler III (1971) Pressure ridge characteristics in the Arctic coastal environment. Proc. 1st Intl. Conf. Port & Ocean Eng. Under Arctic Conditions. Tech. Univ. of Norway, Trondheim, Vol. 1, 152-183.

Williams, E., C.W.M. Swithinbank and G. de Q. Robin (1975) A submarine sonar study of the Arctic pack ice. J. Glaciol, 15(73), pp 349-362.

Wittmann, W.I. and J.J. Schule (1966) Comments on the mass budget of Arctic pack ice. Proc. Symp. Arctic Heat Budget and Atmos. Circ., RAND Corp., Santa Monica, Calif. Report RM-5233-NSF, pp 215-246.

Wolfe, S. and D.P. Hoult (1974) Effects of oil under sea ice. J. Glaciol. 13(69), pp 473-488.